



PCA-F-ShCNNet: Principal Component Analysis-Fused-Shepard Convolutional Neural Networks for lung cancer detection and severity level classification



SK Altaf Hussain Basha ^{a,*}, Pravin R. Kshirsagar ^c, P Srinivasa Rao ^b, Tan Kuan Tak ^d, Dr. B. Sivaneasan ^e

^a Post-Doctoral Research Fellow, Singapore Institute of Technology, Singapore, Professor and Principal, Rishi MS Institute of Engineering & Technology for Women, Hyderabad, India

^b Associate Professor, Department of CSE (Data Science), MVGR College of Engineering (A) Vizianagaram, Andhra Pradesh, India.

^c Professor, Dean (R&D) & HOD (ETC), Department of Electronics & Telecommunication Engineering, J D College of Engineering & Management, Nagpur, India.

^d Associate Professor| Specialist Adult Educator, Electrical Power Engineering Programme, Singapore Institute of Technology, 10 Dover Drive, Singapore 138683.

^e School of Electrical and Electronic Engineering, Singapore Institute of Technology, Singapore

ARTICLE INFO

Keywords:

Cancer

Lung cancer

U-Net

Principal Component Analysis (PCA)

Shepard Convolutional Neural Networks (ShCNN)

ABSTRACT

Lung cancer is one of the leading causes of cancer-related deaths worldwide. Therefore, lung cancer early detection is important to reduce the serious stage by implementing better treatment plans. While chest X-rays are commonly used for lung cancer detection, they are often not sensitive enough to detect early-stage cancers, in previous researches. Hence, to improve detection as well as classify lung cancer severity level, an innovative scheme is developed in this research using the Principal Component Analysis-Fused-Shepard Convolutional Neural Networks (PCA-F-ShCNNet) model, which is obtained by the amalgamation of the Principal Component Analysis Network (PCANet) and Shepard Convolutional Neural Networks (ShCNN). First, the input Computed Tomography (CT) image is pre-processed by utilizing Adaptive Weiner Filtering (AWF) and then, the segmentation is performed using U-Net. Afterwards, lung nodule is identified by employing a grid-based scheme and then a process of feature extraction is performed. Finally, the detection of lung cancer is performed by PCA-F-ShCNNet, where the layers will be modified as well as classification of severity level is executed by employing the same PCA-F-ShCNNet. Additionally, the developed PCA-F-ShCNNet method achieved superior accuracy, F-measure, and precision of 91.566 %, 90.490 % and 92.598 %, when compared to other existing approaches, such as Convolutional Neural Network-based Ebola optimization search algorithm (CNN-EOSA), Wavelet Partial Hadamard Transform-based optimal Support Vector Machine (WPHT-OSVM), Cuckoo Search Optimization, CNN, Local Binary Pattern (CSO + CNN + LBP), multi-round transfer learning and modified Generative Adversarial Network (MTL-MGAN), Improved Deep Neural Network (IDNN), and Grey Wolf Optimization Algorithm and Recurrent Neural Network (GWO + RNN).

1. Introduction

Nowadays, cancer is a worldwide disease and it requires much investment in treatment, research and prevention [1]. In 2020, the Global Cancer Observatory (GLOBOCAN) reported an estimated 19.3 million new cancer cases and around 10 million cancer-related deaths worldwide [2,3]. Cancer is a major health issue and it silently kills millions of people around the world. This disease can spread to all body parts and it affects all age groups [4,5]. In cancer types, lung cancer has the highest

death rate in all other types of cancer [6]. Also, it is the most widespread that causes fatality for both men and women [7]. The lungs are a pair of air-filled organs located in the chest and are the central component of the human respiratory system [8,9].

Lung cancer is a dangerous health concern, which can be effectively detected as well as diagnosed using Artificial Intelligence (AI) systems which are an important progression in the medical field [10]. The alarming surge in lung cancer cases has reached a critical point, prompting an urgent need to detect and diagnose these cases at an

* Corresponding author.

E-mail address: althafbashacse@gmail.com (S.A. Hussain Basha).

earlier stage to effectively combat the disease. The advancement in detecting earlier and recognising lung cancer has significantly enhanced patient outcomes as well as survival rates over the years. Specifically, CT scans have appeared as a valuable device in this regard, providing high-resolution images that enable accurate visualization of internal lung structures, contributing to more effective diagnosis and treatment [11,12]. The CT scans are often chosen over any other medical imaging modalities, visual interpretation of these types of images is time-consuming which may lead to maximising errors as well as delay lung cancer detection [13]. Time series forecasting is crucial in lung cancer detection and monitoring. It aids in early diagnosis, tracks disease progression, and predicts treatment outcomes [14]. Early detection of the condition can significantly reduce mortality rates, but the accuracy of this process is heavily dependent on the availability of skilled operators [15].

Researchers have developed various lung disease diagnostic models aimed at enhancing early-stage detection of lung cancer, providing significant benefits to clinicians and medical professionals [16,17]. With the progress of Computer-Assisted Diagnosis (CAD) and detection techniques, numerous efforts are underway to enhance the clinical effectiveness of lung cancer detection and classification [18]. Lung cancer is feasible to detect through medical imaging checks. Deep learning (DL) approaches are investigated that may be used for detecting, identifying, and forecasting several cancer kinds [19]. CNNs are utilized for video and image classification tasks, although many variants of DL models exist. CNN is especially perfect due to their ability to illustrate data in hierarchical manners that enable to capture and extract complex information from raw data. This enables CNN to accurately classify images, but it exhibits significant variations from the training data, as long as they share common feature characteristics [4–20–21]. Pathologists can benefit from the use of CNN-based methods in the diagnosis of lung cancer, as they may aid in more accurate diagnosis and classification of this disease [19–22]. DL models heavily depend on the extensive use of existing data, with data acquisition being the primary challenge. This issue is more pronounced in medical diagnosis models due to the limited availability of online data [23].

1.1. Problem definition

Lung cancer originates in the lungs, the organs responsible for breathing, and is one of the most common and fatal cancers globally. It develops when abnormal cells in the lungs grow uncontrollably, forming a tumor. Prior studies have explored several approaches for detecting and classifying lung cancer, with the following common challenges:

1. Tumors can vary widely in size, shape, location, and growth patterns. Small tumors or those located in challenging areas of the lungs may be difficult to detect or classify accurately in most of the existing research.
2. Previous models for lung cancer detection often required substantial computational resources, limiting their implementation in resource-constrained settings like smaller hospitals or clinics.
3. Combining data from different imaging modalities required complex fusion techniques, and poor data integration often led to suboptimal performance in past research.

The challenges outlined above motivate the development of the PCA-F-ShCNNNet model for lung cancer severity classification and detection. Moreover, the PCA-F-ShCNNNet is developed by combining PCANet and ShCNN. PCANet is a feature extraction technique that reduces data dimensionality, making it efficient for large-scale medical imaging. It can be adapted to different lung cancer detection modalities by adjusting the input or PCA components and integrates multimodal data to improve prediction accuracy by incorporating comprehensive patient information. Subsequently, the ShCNN offers flexibility across various imaging techniques, enhancing generalization in lung cancer detection.

It can also integrate multimodal data, efficiently combining features from diverse sources for better detection and predictions. Additionally, ShCNN supports context-aware feature extraction, learning spatial dependencies to improve robustness against noise and subtle variations in detecting early lung cancer signs. By leveraging the advantages of both PCANet and ShCNN models, the integrated system becomes more capable of handling complex, noisy, and multimodal medical data while delivering more accurate and interpretable predictions. This combination leads to improved robustness, generalization, detection accuracy, and computational efficiency for lung cancer severity level classification and detection.

1.2. Research contribution

The contribution of this research,

1. **PCA-F-ShCNNNet model to detect lung cancer and classify its severity level:** This research introduces the PCA-F-ShCNNNet model for classifying and detecting lung cancer severity.
2. First, lung lobe segmentation is performed by U-Net, and lung nodules are identified through a grid-based approach.
3. Finally, lung cancer and detection severity classification are performed by the PCA-F-ShCNNNet model, which combines the PCANet and ShCNN models.

1.3. Organization

The remaining sections are organized as: Section 2 explains a literature review of previous models. Section 3 details the developed method. The estimation of the model's output is discussed in Section 4. Finally, Section 5 provides the conclusion of the research.

2. Literature review

Mohamed, T.I., et al. [3] developed the CNN-based EOSA for Lung cancer detection and severity level classification. This model provided an effective digital image of lung structure, also it enhanced the decision-making of treatment for patients. However, it did not contain an insufficient size of data sample and it had time complexity because of limited resources. Venkatesh, C., et al. [7] devised the CSO + CNN + LBP to classify severity levels and detect Lung cancer. This technique effectively learned features and complex patterns in the CT images. However, it was not able to improve the lung's structure in another type of imaging modality. Althubiti, S.A., et al. [24] introduced Ensemble Learning Framework with Gray Level Cooccurrence Matrix (GLCM) for Lung cancer detection and severity level classification. The model was capable of providing advanced applications in medical computer-aided diagnosis for lung cancer. Yet, this model did not have the power to analyze and detect the larger number of datasets. Shakeel, P.M., et al. [25] established an IDNN and ensemble classifier to detect Lung cancer and classify severity levels. The model has effectively reduced dimensionality since it employs the approximation concept and spiral settings, which efficiently choose optimized features. Still, the method consumed a huge time to detect cancer because of its high dimension.

Gujjan, V.K., et al. [15] devised the GWO + RNN for Lung cancer detection and severity level classification. This approach prevented overfitting, where the model memorized training instances instead of learning meaningful patterns. It did not include AI techniques, which help to analyze the disease diagnosis and patient risk identification. Suganya, V., et al. [16] introduced the Lion-Butterfly Optimization (LBO) based Stacking Ensemble Learning Classification (SELC) Model to detect Lung cancer and classify severity level. This scheme ensured that only relevant features were used and prevented the model from fitting noise in the image. This module neglected to analyze by comparing the behaviors of cancers and non-cancers. Wankhade, S. and Vigneshwari, S., [18] established the 3D-CNN for Lung cancer classification and

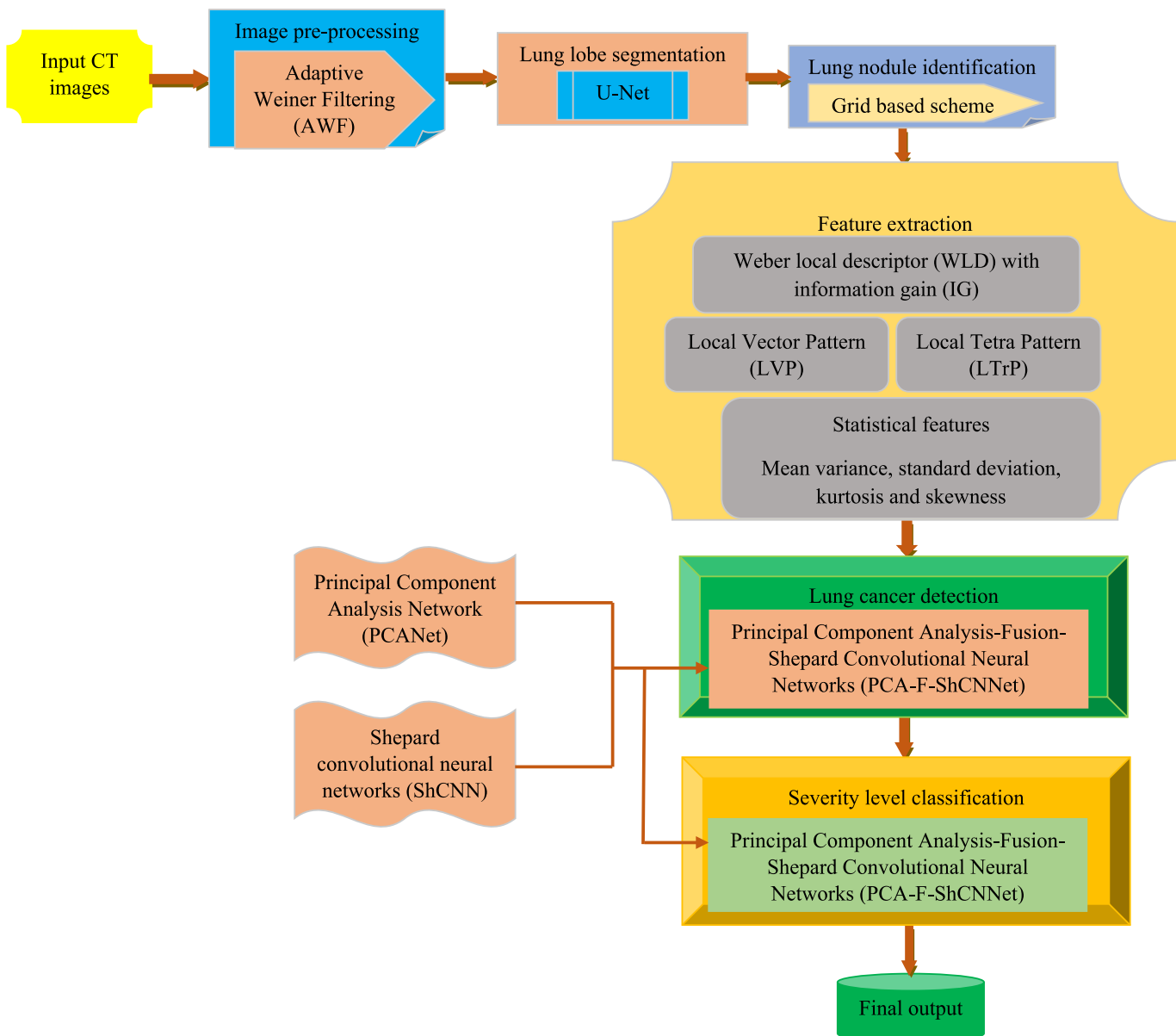


Fig. 1. Diagrammatic representation of proposed Principal Component Analysis-Fused-Shepard Convolutional Neural Networks (PCA-F-ShCNNNet) for the classification and detection of the severity level of lung cancer.

detection. This model reduced the dimensionality of extracted features while preserving essential information and it was effectual without sacrificing predictive power. However, it did not enhance the DL model's comprehensibility and failed to apply adequate high-quality training data. Tiwari, A., et al. [19] developed the RNN- Generative Adversarial Network (GAN) to classify and detect Lung cancer. The model effectively enabled the consecutive process for lung cancer images as well and it created a realistic tumor sample to combine the strengths of GAN and RNN. However, it was difficult to real-time mechanism since the Gaussian filters and RNN-GAN required the highest computational cost. Venkatesan N et al. [26] presented a WPHT-OSVM for the detection of lung cancer. The pre-processing was performed with an adaptive median filter, and the Improved Weight-Based Beetle Swarm (IW-BS) algorithm was used to tune the SVM parameters, enhancing kernel performance. However, the model had high processing time and memory demands. Y Luo et al. [5] presented a multi-round transfer learning and modified GAN (MTL-MGAN) algorithm for lung cancer detection. In this work, the MTL was used to optimize knowledge

transfer between source and target domains. Moreover, this model generated additional training data with the MGAN, leading to enhanced model performance across multiple datasets. However, this model required significant processing memory and power.

2.1. Challenges

The challenges faced while reviewing former modules of detection and classifying lung cancer severity levels are discussed below:

1. The scheme EOSA-CNN introduced in [3] helps reduce the false positive rate efficiently. Nevertheless, it did not utilize over-sampling and cluster-based over-sampling techniques and did not incorporate huge sample sizes to enhance model performance.
2. In [7], the devised model was capable of adapting different types of CT images and different types of lung cancer. However, it required a large amount of labeled CT images dataset to train and validate the neural network.

3. The model in [25] reduced the time complexity. However, the developed algorithm required a huge number of computational resources because of the high complexity as well as the large size of medical images used in this model.
4. The early detection of lung cancer is required to protect human lives. To diagnose this, a CT scan is one of the primary modalities. However, the manual analysis of CT scans is not accurate and it consumes a lot of time. By considering these types of issues, the DL-based models are used to accelerate the better detection of CT scans into cancerous and non-cancerous.

3. Materials and methods

3.1. Materials

This section describes the datasets such as the LIDC-IDRI database and Iraq-Oncology Teaching Hospital/National Center for Cancer Diseases (IQ-OTH/NCCD)- Lung Cancer Dataset. Moreover, the proposed PCA-F-ShCNNet model is evaluated using certain parameters, like F-measure, accuracy, and precision.

3.1.1. LIDC-IDRI database

This dataset [27] includes thousands of high-resolution chest CT scans, each comprising a series of 2D slices that help visualize lung structures and nodules. It is typically split into training, test sets, and validation. In this study, 1,433 images are utilized for detection and severity classification, with 90 % allocated for training and 10 % for testing. Moreover, the size of this dataset contains 2,103 images, with 794 labeled as normal and 1,309 as abnormal cases.

3.1.2. IQ-OTH/NCCD- lung cancer Dataset

This database [28] comprises 1190 CT scan images from 110 cases, which are classified into three categories: normal (55 cases), benign (15 cases), and malignant (40 cases). Each CT scan includes 80 to 200 slices, depicting various views of the chest. The cases vary in age, occupation, education, gender, and residence, primarily from central Iraq, including Salahuddin, Wasit, Diyala, Baghdad, and Babylon. The scans were originally in DICOM format. Additionally, the total size of the dataset is 1096, with 416 labeled as normal and 680 as abnormal cases.

3.2. Methods

In 2018, lung cancer is the most threatening disease that has an effect on men as well as women and it accounts for total cancer death of 18.4 %. In recent times, the treatment has significantly enhanced the survival time for a particular group of patients. However, lung cancer still requires a lot of improvement, specifically in early detection and screening. The major intention of this exploration is to design an innovative scheme based on lung cancer detection and severity level classification using PCA-F-ShCNNet. Here, PCA-F-ShCNNet is obtained by the amalgamation of PCANet [13] and ShCNN [29]. Initially, the input CT image was obtained from the database [27]. The input CT is pre-processed by utilizing AWF [30] to avoid redundant noise. Then, the pre-processed image is segmented using U-Net [30]. Afterwards, lung nodule is identified by employing a grid-based scheme and then a feature extraction process is carried out. Here, the extracted features are Weber local descriptor (WLD) [31] with Information gain (IG) [32], Local Vector Pattern (LVP) [33], Local Tetra Pattern (LTrP) [34] and statistical features [1] like kurtosis, variance, standard deviation, mean, and skewness. At last, the detection of lung cancer is successfully done using PCA-F-ShCNNet, where the layers are modified as well as lung cancer severity level is classified by developing PCA-F-ShCNNet. Fig. 1 shows the block diagram of the detection and classification of the severity level of Lung cancer using PCA-F-ShCNNet.

3.2.1. Acquisition of image

Let us consider, that the input CT image is taken from the Lung Image database U that comprises e the amount of CT lung images, which is defined as

$$U = \{U_1, U_2, \dots, U_x, \dots, U_e\} \quad (1)$$

Here, the total number of CT images is given as e , U_x indicates the x^{th} number of CT images and this image is given as input image for detecting and classifying lung cancer severity level in this research.

3.2.2. Pre-processing using AWF

It is an essential process that helps to improve the quality of a given image and correct any other artifacts or distortions in the image. Here, U_x is taken as an input image for pre-processing, where the pre-

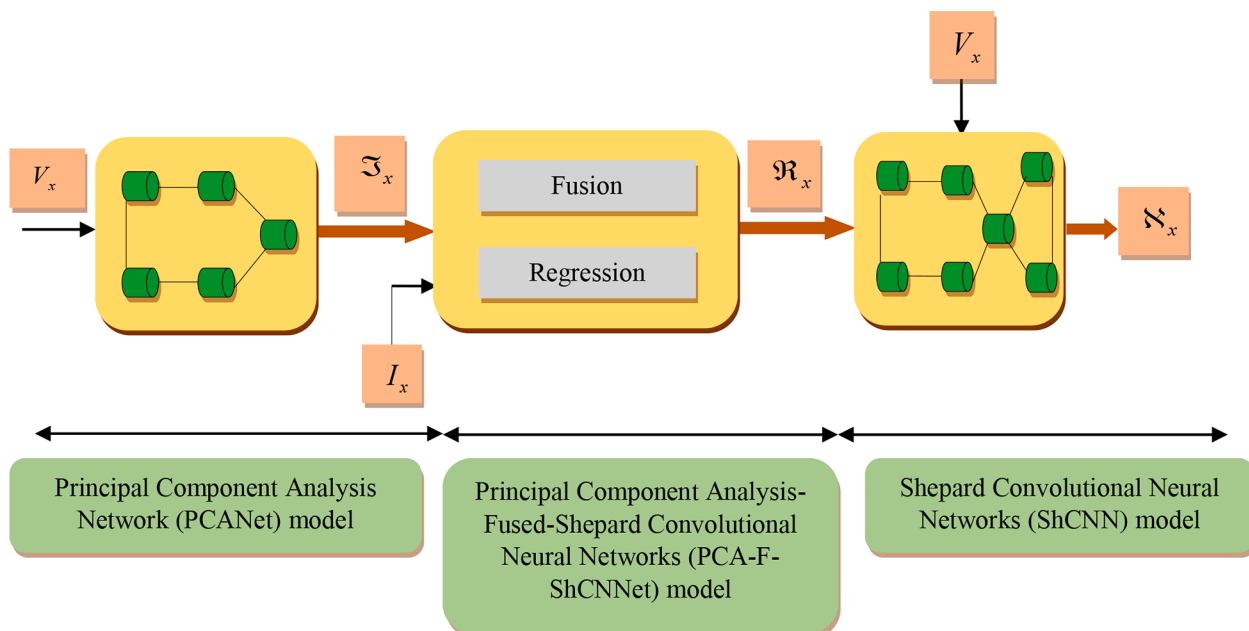


Fig. 2. General outline for Principal Component Analysis-Fused-Shepard Convolutional Neural Networks (PCA-F-ShCNNet) model by combining Principal Component Analysis Network (PCANet) model and Shepard Convolutional Neural Networks (ShCNN).

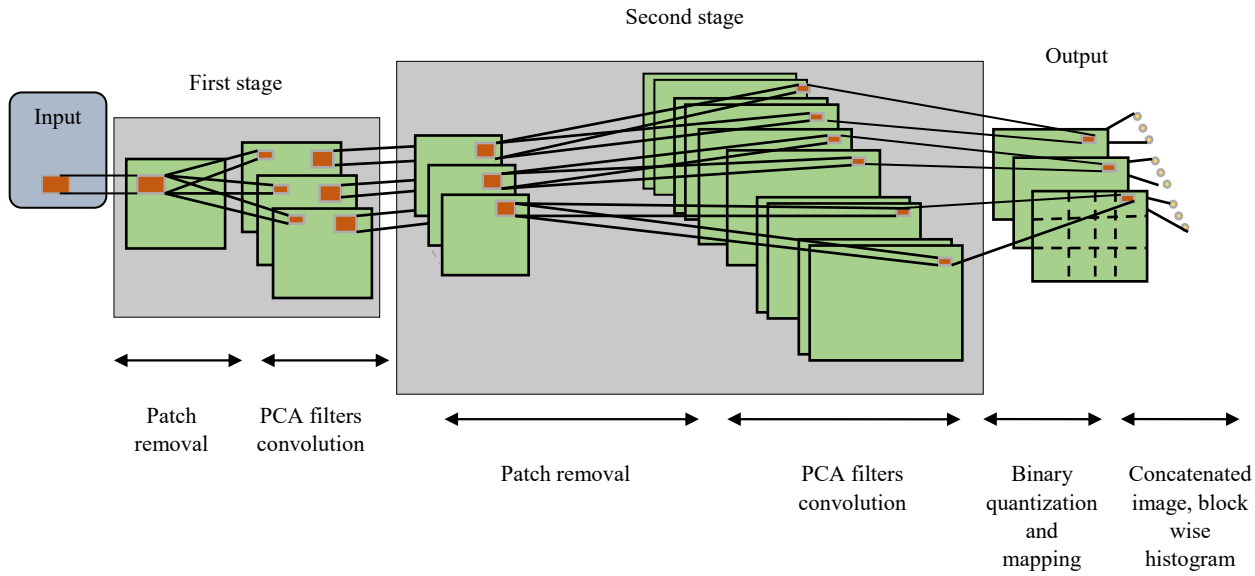


Fig. 3. The architecture of the Principal Component Analysis Network (PCANet) utilized for the lung cancer detection.

processing is performed using AWF [35]. This filtering is effective since it preserves high-frequency parts and edges in the image. Therefore, the AWF is given as,

$$D(p', q') = \zeta + (1 - j' + \Delta) * (H(p', q') - \zeta) \quad (2)$$

$$j' = \frac{h_{avg}}{h_{var} + 1} \quad (3)$$

$$\Delta = \frac{h_{var}}{h_{avg} + h_{max} + 1} \quad (4)$$

Here, $H(p', q')$ is given as the original pixel and output pixel. Then mean of variance sum of every pixel in the selected window is illustrated as h_{avg} and h_{var} is denoted as the variance of the current pixel. The highest variance of every pixel in the image is specified as h_{max} . Therefore, the acquired result from the preprocessing phase is considered as V_x .

3.2.3. Lung lobe segmentation by u-net

Identifying and separating the different types of lobes from the lung using a CT scan is known as lung lobe segmentation. This process utilizes preprocessed images V_x and the process of lobe segmentation is done on U-Net [30]. This framework effectively minimized the computation complexity of segmentation. Also, it easily adapts to various types of medical imaging. Moreover, the architecture of U-Net and its description are provided below in the reference (a appendix) section.

3.2.4. Lung nodule detection using grid-based scheme

Lung nodule detection is used to classify and diagnose small abnormal growths or lesions in the lungs by using medical imaging like CT scans or MRIs. This growth is represented as malignant (cancerous) or benign (non-cancerous) as well and the early detection helps to determine the best course of treatment. Here, the obtained segmented outcome W_x is given in the identification of lung nodules, where it is carried out using a grid-based scheme. A grid-based scheme [33] is employed to separate the position of segments into several blocks that are called grids. To make computation simple, minimize the time of computation, and also improves the detection accuracy, the process segments the images into different blocks. Thus, the position of the nodule is discovered and it is derived as X_x .

3.2.5. Feature extraction

It is an essential process to extract and identify relevant details that

characterize each class. Here, the extracted features are, WLD with information gain, LVP, LTrPs and statistical features. Therefore, the segmented lung lobe W_x is given for the feature extraction process as an input.

3.2.5.1. WLD with information gain. The WLD [31] feature is formed based on two fundamentals, like differential excitation ω and orientation ν .

— **Differential excitation:** The micro-variation in an image is generated as account intensity dissimilarity among neighboring pixels, which is described as,

$$AL = \sum_{c=0}^{t'-1} AL(\kappa_c) = \sum_{c=0}^{t'-1} L(\kappa_c) - L(\kappa_{n'}) \quad (5)$$

Here, c^{th} neighbor $\kappa_{n'}$ specifies $\kappa_c (c = 0, 1, \dots, t' - 1)$ and t' implies the overall amount of neighbors in a region. $L(\kappa_c)$ represents the neighbored pixel intensity and the intensity of the present pixel is given as $L(\kappa_{n'})$. Then it is expressed as,

$$\omega(\kappa_{n'}) = \arctan\left(\frac{AL}{L}\right) = \arctan\left(\sum_{c=0}^{t'-1} \left(\frac{A(\kappa_c) - A(\kappa_{n'})}{A(\kappa_c)} \right) \right) \quad (6)$$

If $\omega(\kappa_{n'})$ is positive, center pixel appears darker compared to its neighboring pixels, $\omega(\kappa_{n'})$ is negative, then the present pixel is lighter concerning neighbor pixels.

— **Orientation:** It specifies the directional property of the pixel that is denoted as,

$$\nu(\kappa_{n'}) = \arctan\left(\frac{PL_g}{PL_\lambda}\right) \quad (7)$$

Thus, $PL_g = L(\kappa_7) - L(\kappa_3)$ and $PL_\lambda = L(\kappa_5) - L(\kappa_1)$ is measured from two types of filters. By using two values, the image descriptor for the WLD histogram is computed by,

$$P_{x',y',z'} = \sum_{m'} \wp(S_{m'} = S), \left(S_{m'} = \begin{bmatrix} \wp_m - \theta_{x',o} & 1 \\ \frac{\wp_{x',w'} - \theta_{y',o}}{S} & 2 \end{bmatrix} \right) \quad (8)$$

Hence, x' ranges \wp_m and quantized orientation index implies y' , here, the IG is applied with WLD.

IG [32] calculates the number of information in bits concerning class recognition. Moreover, it evaluates predictable reduction in entropy as,

$$IG(N_v, v_h) = T(N_v) - \sum_{Z=\text{value}(N_h)}^{\frac{|N_h| - \ell}{|N_v|}} T(N_{v_h=\ell}) \quad (9)$$

$$T(N) = -Y + (N)\log_2 Y + (N) - Y - (N)\log_2 Y(N) \quad (10)$$

where, training sample probability in set N specifies positive or negative class, which represents $Y \pm (N)$. Therefore, WILD with IG is specified as FF_1 .

3.2.5.2. LVP. LVP [34] technique is employed to analyze spatial relationships among micropatterns with various orientations and spatial dimensions, as well as the interactions among the entire pixel and its neighbors. The range between adjacent pixels and their target is calculated to determine the optimal directions for producing pixels, and the resulting information is used to eliminate irrelevant and unnecessary features. This is specified as A_3 .

3.2.5.3. LTrP. The LTrP [34] is an image retrieval method that encodes relationships between neighborhoods and referenced pixels using high-order derivative directions, offering a general comparison between the referenced pixel and its neighbors to capture micropatterns in local sub-regions. Therefore, the LTrP is derived as,

$$A_4(E_r) = \left\{ \begin{array}{l} p_3(T_{Dir}^{i-1}(E_1, H), T_{Dir}^{i-1}(E_r)), \\ p_3(T_{Dir}^{i-1}(E_2, H), T_{Dir}^{i-1}(E_r)), \dots, \\ p_3(T_{Dir}^{i-1}(E_O, H), T_{Dir}^{i-1}(E_r)) \end{array} \right\} |O = 1, 2, \dots, O : H = 1 \quad (11)$$

Here, the LTrP is denoted as A_4 .

Thus, the texture feature is formulated as follows,

$$TF = \{A_3, A_4\} \quad (12)$$

3.2.5.4. Statistical features. It is used to analyze, accumulate and review images to make an effective decision. The statistical features applied in

this model are described below,

a) Mean

The mean [36] indicates the sum of total pixels and dividing it by the total amount of pixels in the image that is designated as,

$$G_1 = \sum_{gg=0}^{ss-1} V_x * E(V_x) \quad (13)$$

Here, mean refers G_1 , $E(V_x)$ denotes the input image probability, gg shows the gray level image and ss refers to total gray level images.

b) Variance

It [36] specifies the dissimilarity in gray images based on the mean and it measures how each pixel deviates from the mean value that is considered as,

$$G_2 = \sum_{gg=0}^{ss-1} (V_x - G_1) * E(V_x) \quad (14)$$

Here, variance is described as G_2 .

c) Standard deviation

Standard Deviation (SD) [36] represents the deviation value of the image grey level related to the mean grey level. Here, SD indicated as,

$$G_3 = \sqrt{\sum_{gg=0}^{ss-1} (V_x - G_2)^2 * E(V_x)} \quad (15)$$

Here, the standard deviation is specified as G_3 .

d) Kurtosis

This [36] measures the levelling of a distribution with relation to a normal distribution that is resolute by,

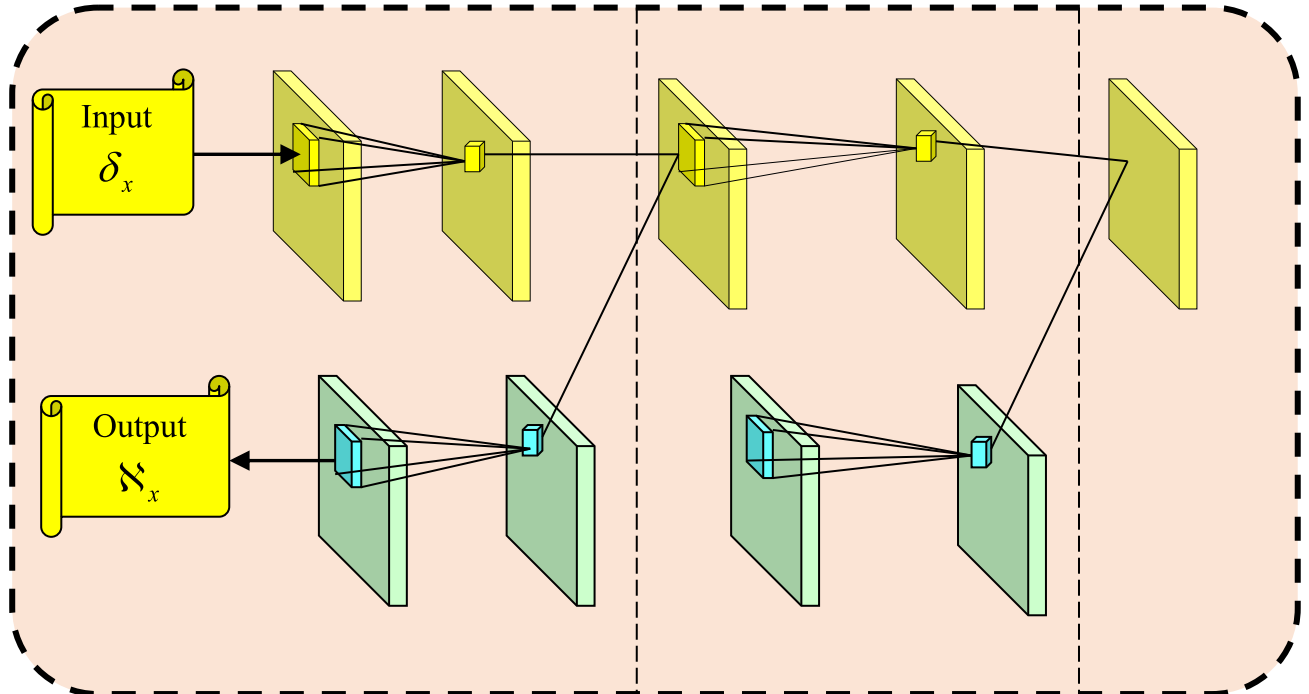


Fig. 4. Structure of Shepard Convolutional Neural Networks (ShCNN) Model used to detect lung cancer.

$$G_4 = G_3^{-4} \left[\sum_{V_x=0}^{ss-1} (V_x - G_3)^4 * E(V_x) \right] \quad (16)$$

Here, kurtosis is implied as G_4 .

e) Skewness

It [36] refers to the extent distribution of a specific feature deviates from symmetry around its mean value that is resolute by,

$$G_5 = G^{-3} \left[\sum_{V_x=0}^{ss-1} (V_x - G_3)^3 * E(V_x) \right] \quad (17)$$

Thus, skewness is defined as G_5 . Therefore, the texture feature is employed in statistical features to obtain a feature vector that is derived as,

$$FF_2 = \{G_1, G_2, G_3, G_4, G_5\} \quad (18)$$

Hence, the feature vector obtained by the extracted feature is given as follows,

$$I_x = \{FF_1 \| FF_2\} \quad (19)$$

3.2.6. Lung cancer detection using PCA-F-SHCNNNet using CT image

The lung cancer detection process is used to detect and diagnose lung cancer earlier, when the disease is at the treatable level and make survival rate is higher. However, the symptoms of lung cancer are not noticeable and it did not show any symptoms in the early stage that make it complex. So far, different types of traditional models have been available to detect lung cancer but, these methods are not capable of differentiating between benign and malignant lesions and they require additional testing. Therefore, an innovative method is proposed namely, PCA-F-SHCNNNet for lung cancer detection which is a hybridization of the PCANet model and SHCNN. Initially, the pre-processed image V_x is given as the input to the PCANet model to get the outcome, which is denoted as \mathfrak{J}_x . After that, the previous output \mathfrak{J}_x along with the extracted feature I_x is considered as input $\lambda_x \in \{\mathfrak{J}_x, I_x\}$ and it is subjected to the PCA-F-SHCNNNet model. The PCA-F-SHCNNNet includes fusion and regression process, thus, the attained result is specified as \mathfrak{R}_x . Then, the obtained output from the previous model \mathfrak{R}_x and the pre-processed image V_x is defined as an input, such that $\delta_x \in \{\mathfrak{R}_x, V_x\}$ is fed into the SHCNN model to attain detected output. Hence, the detected outcome is specified as \mathfrak{N}_x . The general outline for PCA-F-SHCNNNet is illustrated in Fig. 2.

3.2.6.1. PCANet model

The PCANet [13] is a statistical technique for feature extraction that reduces data dimensionality. It is adaptable to various imaging modalities for lung cancer detection by adjusting the input layer or PCA components. Additionally, PCANet can integrate data from different sources, learning principal components separately and combining them to enhance prediction accuracy by incorporating more comprehensive patient information. Particularly, the PCANet includes only a cascade linear map that is followed using block histograms and binary hashing but now it is manageable for mathematical analysis as well as to validate its effectiveness. This evaluation conducts essential theoretical insights into inclusive deep networks.

Let us consider J the amount of input training images $\{V_x\}_{x=1}^J$ with size $[g \times h]$, then patch size is considered as $[b_1' \times b_2']$ in every stage. The architecture of PCANet is specified in Fig. 3 and the PCA filters learn from the input image $\{V_x\}_{x=1}^J$ and all the components are presented much more effectively. The PCANet has three stages that are evaluated as follows,

a) First Stage: PCA.

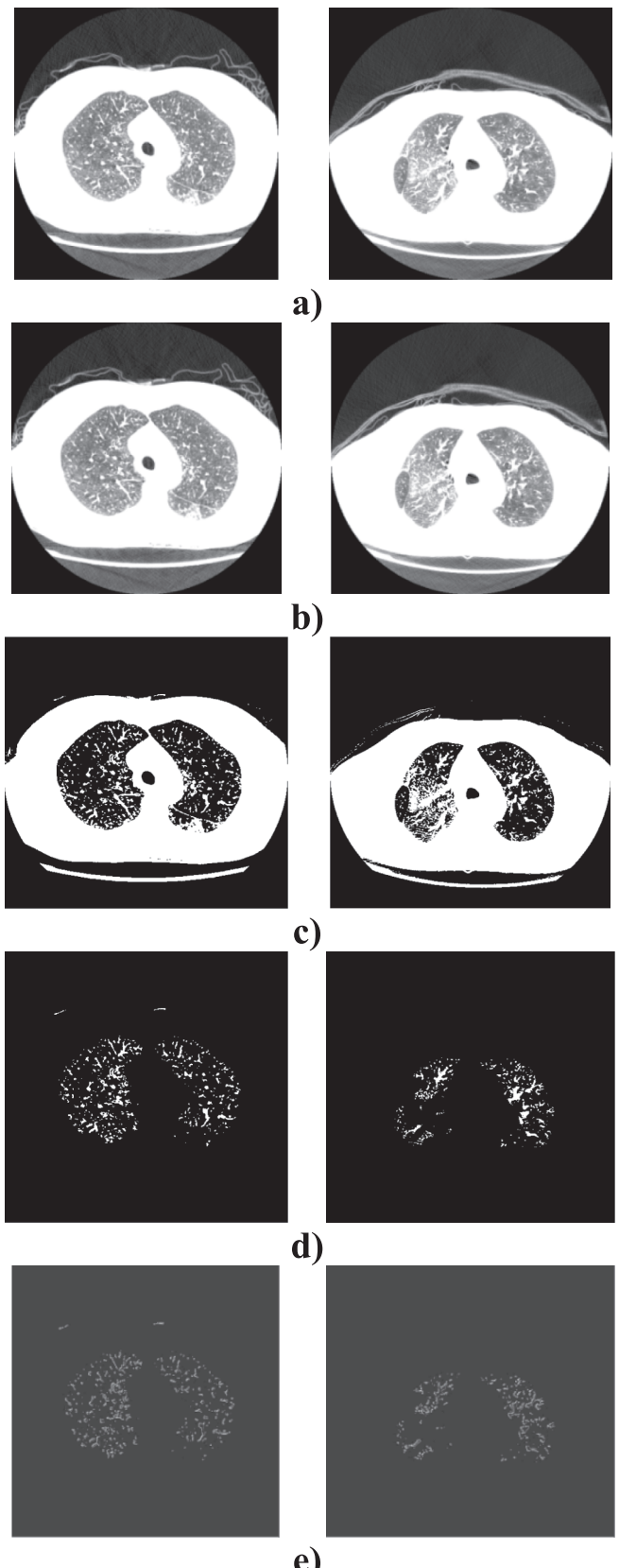


Fig. 5. The experimental outcome of the proposed model for the LIDC-IDRI database, a) Input images, b) Images of Pre-processing, c) Images of Segmentation, d) Lung nodule images, e) Feature extracted images.

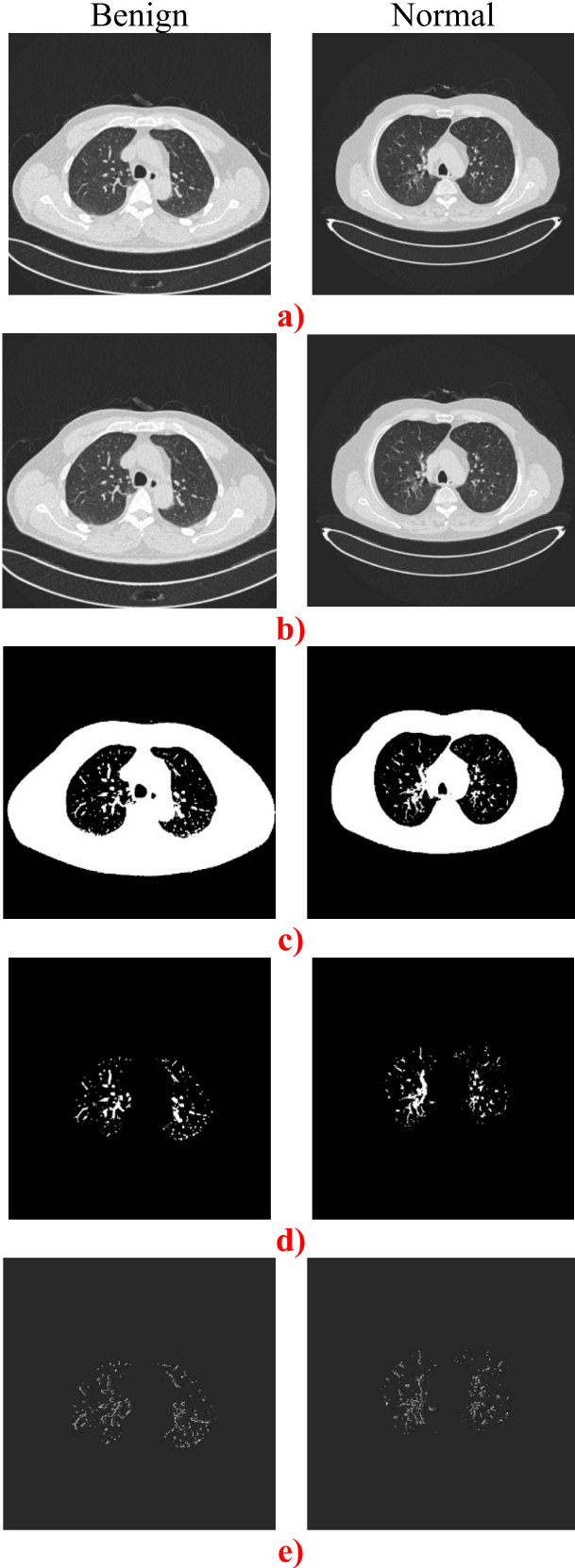


Fig. 6. Experimental results of the developed model based on IQ-OTH/NCCD – Lung Cancer Dataset, a) Input images, b) images of pre-processing, c) images of segmentation, d) Lung nodule images, e) images of extracted feature.

Assume $[b' \times b'_2]$ a patch around every pixel and it collects every patch of x^h image, which is represented as $k_{x,1}, k_{x,2}, \dots, k_{x,y} \in R^{b_1 b_2}$, here all $k_{x,s}$ represents s^{th} vectorized patches in V_x . In every patch, the mean patch is subtracted and attained as $\bar{E}_x = \{\bar{k}_{x,1}, \bar{k}_{x,2}, \dots, \bar{k}_{x,y}\}$, while $\bar{k}_{x,s}$ denotes the mean-removed patch. Evaluating the matrix for the input image is given as,

$$E = [\bar{E}_1, \bar{E}_2, \dots, \bar{E}_J] \in R^{b'_1 b'_2 \times J_y} \quad (20)$$

Assume, the amount of filter in x^h layer is Z_x , reconstruction error is minimized by PCA in orthonormal filters as

$$\min_{A \in R^{b'_1 b'_2 \times Z_x}} \|E - AA^\top E\|_N^2, \quad (21)$$

Likewise,

$$A^\top A = R'_{Z_1} \quad (22)$$

Therefore, R'_{Z_1} indicates the identified matrix with size $[Z_1 \times Z_2]$. The solution is specified as Z_1 and the principal eigenvectors are denoted as EE' . Hence, the PCA filter is formulated as,

$$P_h^1 = \text{mat}_{b'_1 b'_2}(F_h(EE')) \in R^{b'_1 \times b'_2}, h = 1, 2, \dots, Z_1, \quad (23)$$

Thus, the $\text{mat}_{b'_1 b'_2}(K')$ is function that connected with $K' \in R^{b'_1 b'_2}$ to matrix $P \in R^{b'_1 \times b'_2}$ and $F_h(EE')$ specifies h^{th} principle eigenvector of EE' . The important variation of every mean extracted training patch is captured by the main principal eigenvectors.

b) Second phase: PCA.

By repeating the corresponding process in the first stage, assume h^{th} filter outcome of the first stage is defined as,

$$V_x^h = V_x * P_h^1, x = 1, 2, \dots, J \quad (24)$$

Here, $*$ indicates the 2D convolution and V_x boundary is zero-padded before convolving through P_h^1 to produce V_x^h with same dimension V_x .

Here, overlapping patches V_x^h are gathered from the first phase, which subtracts the average of the patch from every patch and generated $\bar{G}_x^h = [\bar{S}_{x,h,1}, \bar{S}_{x,h,2}, \dots, \bar{S}_{x,h,y}] \in R^{b'_1 b'_2 \times y_1}$ here $\bar{S}_{x,h,s}$ implies s^{th} average of neglected patch of V_x^h filter output and concatenate G^h for entire resultants of filter is computed by,

$$G' = [G'^1, G'^2, \dots, G'^{Z_1}] \in R^{b'_1 b'_2 \times Z_1 J_q} \quad (25)$$

In the second stage, the PCA filters are attained by,

$$P_\varepsilon^2 = \text{mat}_{b'_1 b'_2}(F_\varepsilon(EE')) \in R^{b'_1 \times b'_2}, \varepsilon = 1, 2, \dots, Z_2 : \quad (26)$$

For all the input V_x^h in the second stage, the output Z_2 is attained, the every convolves V_x^h through P_ε^2 for $\varepsilon = 1, 2, \dots, Z_2$.

$$I_x^h = \{V_x^h * P_\varepsilon^2\}_{\varepsilon=1}^{Z_2} \quad (27)$$

The amount of outcome from the second stage is referred to as Z_1, Z_2 .

c) Output phase

For all Z_1 input images V_x^h in the second phase, that has Z_2 real-valued outcomes $\{V_x^h * G_\varepsilon^2\}_{\varepsilon=1}^{Z_2}$ from the second stage. These outcomes are binarized and attained $\{N(V_x^h * G_\varepsilon^2)\}_{\varepsilon=1}^{Z_2}$, hence $N(\cdot)$ specifying the Heaviside step function, but the value is one positive or zero.

The vector of Z_2 binary bits around all pixels is a decimal number that transforms Z_2 the outcome I_x^h back into the single integer-valued image that is illustrated as,

$$Z_x^h = \sum_{\varepsilon=1}^{Z_2} 2^{\varepsilon-1} N(V_x^h * G_\varepsilon^2) \quad (28)$$

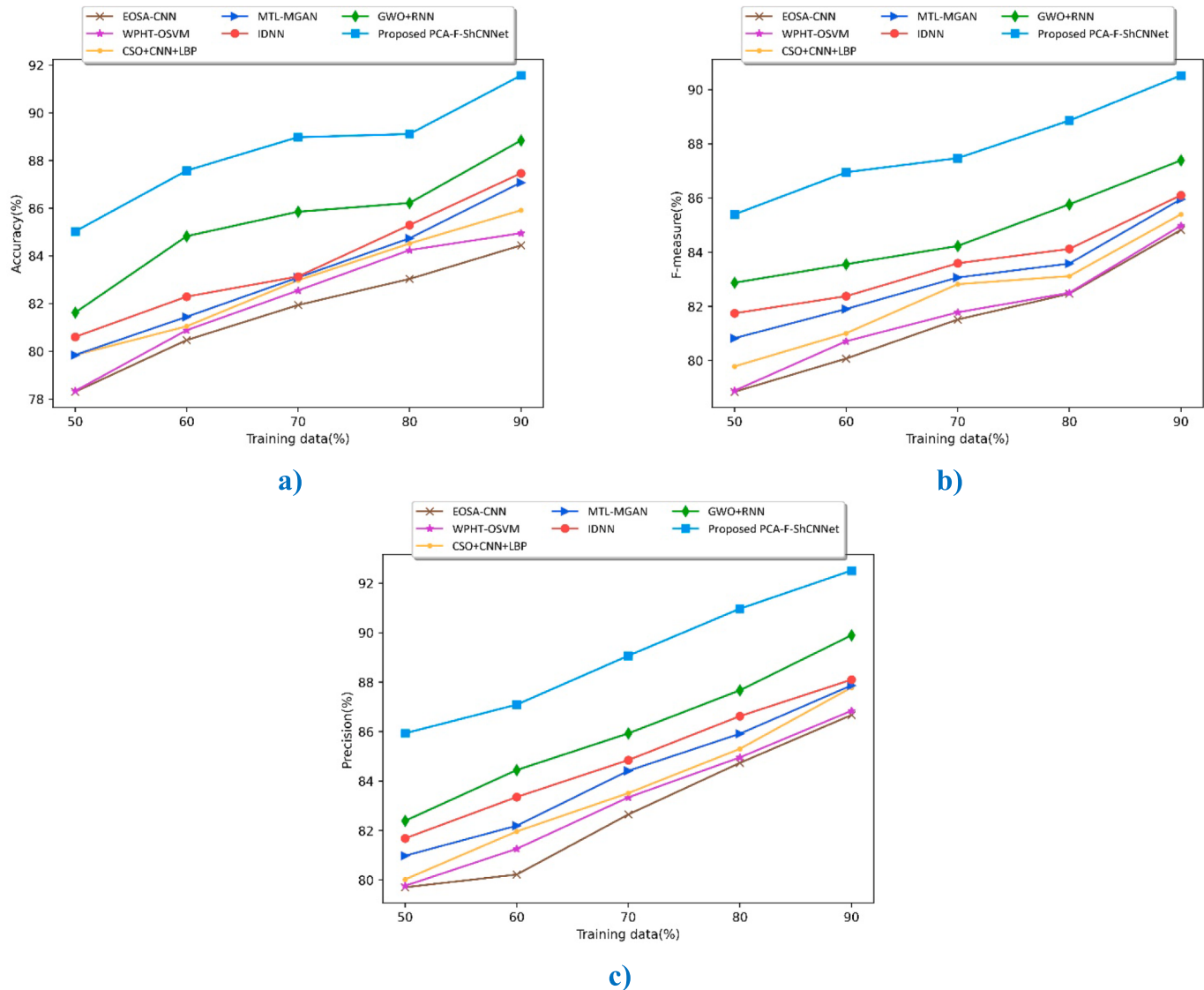


Fig. 7. Evaluation concerning learning data for first-level classification for the proposed model, a) accuracy, b) F-measure, c) Precision.

Thus, every integer in the interval of $[0, 2^{Z_2} - 1]$. For Z_2 outcome, the weights and orders are irrelevant.

For all Z_1 images $Z_x^h \hbar = 1, \dots, Z_1$, The histogram of decimal values in every block as well as concatenates entire Φ histograms into one vector, which is given as $Bhist(I_x^h)$. Once encoding is done, a feature of input V_x is formulated as a set of block-wise histograms that is determined by,

$$\mathfrak{I}_x = [Bhist(I_x^1), \dots, Bhist(I_x^{Z_1})]^T \in R^{(2^{Z_2})Z_1\Phi} \quad (29)$$

Here, the input image indicates V_x and outcome of PCANet is signified as \mathfrak{I}_x . The general architecture of PCANet is expressed in Fig. 3.

3.2.6.2. Pca-f-shcnnnet model

The proposed PCA-F-ShCNNNet model is developed to classify severity levels and detect lung cancer, which is the integration of the PCANet [13] model and the ShCNN [29] method. Here, PCA-F-ShCNNNet attains the outcome from the PCANet model \mathfrak{I}_x , extracted feature I_x also, performs fusion as well as regression function. The regression model compares the similarities between target features and extracted features.

Finally, it obtained the output as \mathfrak{R}_x .

By considering the fusion,

$$Y = \sum_{v=1}^{GG} (I_x)_v * \zeta_v \quad (30)$$

Here, weight is referred to as ζ and several feature vector is given as GG and Y imply the outcome from t^{th} interval and I_x specifies feature vector.

By applying Fractional Calculus (FC),

$$\mathfrak{R}_x = nY + \frac{1}{2}nY_1 \quad (31)$$

where, n is defined as constant.

Let us consider,

$$\mathfrak{R}_x = n \sum_{v=1}^{GG} I_{xv} * \zeta_v + \frac{1}{2}n\mathfrak{I}_x \quad (32)$$

$$\mathfrak{R}_x = n \sum_{v=1}^{GG} I_{xv} * \zeta_v + \frac{1}{2}n[Bhist(I_x^1), \dots, Bhist(I_x^{Z_1})]^T \in R^{(2^{Z_2})Z_1\Phi} \quad (33)$$

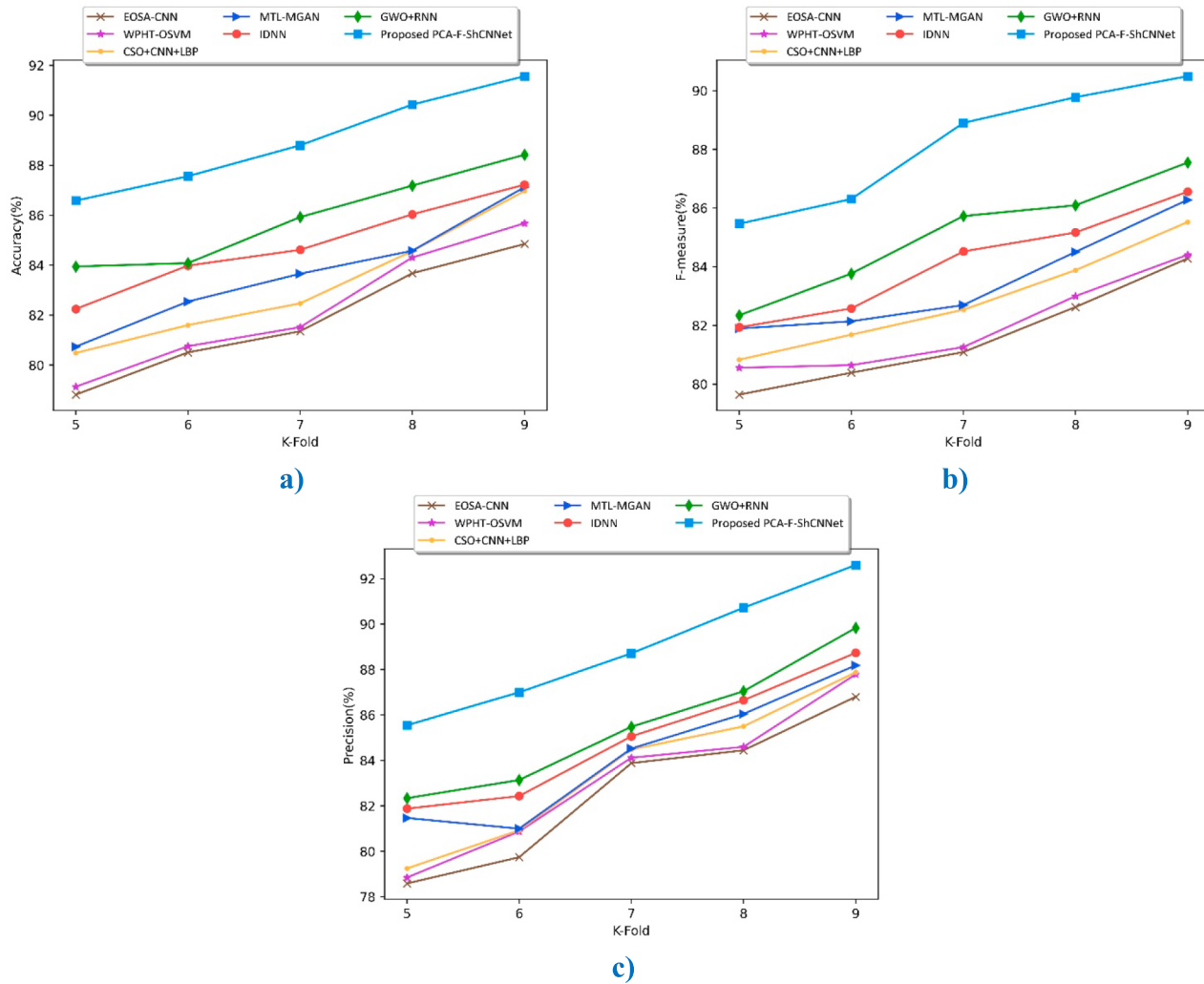


Fig. 8. Estimation based on K-fold for first-level classification using Principal Component Analysis-Fused-Shepard Convolutional Neural Networks (PCA-F-ShCNNNet), a) accuracy, b) F-measure, c) Precision.

Here, $\sum_{v=1}^{GG} I_{xv} * \zeta_v \leftarrow Y'$ and $[Bhist(I_x^1), \dots, Bhist(I_x^{Z_1})]^T \in R^{(2^{Z_2})Zl1\Phi} \leftarrow Y'$. Hence, the attained outcome from PCA-F-ShCNNNet is illustrated as \mathfrak{N}_x .

3.2.6.3. ShCNN model

ShCNN [29] is referred to as a neural network and it is entirely equal to the CNN model but, it does not have a ReLU layer. This model helps to process the pixel data and it can automate the imperative features without human intervention. Additionally, the ShCNN offers flexibility in adapting to various medical imaging modalities, improving generalization across different techniques used in lung cancer detection. It can also integrate multimodal data, efficiently aggregating features from diverse sources to enhance detection and provide more comprehensive

predictions. Additionally, ShCNN enables context-aware feature extraction, learning spatial dependencies and context from surrounding regions, making it more robust to noise and subtle variations for detecting early signs of lung cancer. The ShCNN offers effective outcomes and it is easy to implement also, it has an understandable structure. The general architecture of the ShCNN model is represented in Fig. 4.

The Shepard's approach is re-written in a convolution form, which is expressed by,

$$\mathfrak{N}_x = \begin{cases} (B * \mathfrak{N}_x)_{uu} / (B * K)_{uu} & \text{if } K_{uu} = 0 \\ \mathfrak{N}_x & \text{if } K_{uu} = 1 \end{cases} \quad (34)$$

Therefore, the equation becomes,

$$\mathfrak{N}_x = \begin{cases} \left(B * n \sum_{v=1}^{GG} \Psi_v * \zeta_v + \frac{1}{2} n [Bhist(I_x^1), \dots, Bhist(I_x^{Z_1})]^T \in R^{(2^{Z_2})Zl1\Phi} \right)_{uu} / (B * K)_{uu} & \text{if } K_{uu} = 0 \\ n \sum_{v=1}^{GG} \Psi_v * \zeta_v + \frac{1}{2} n [Bhist(I_x^1), \dots, Bhist(I_x^{Z_1})]^T \in R^{(2^{Z_2})Zl1\Phi} & \text{if } K_{uu} = 1 \end{cases} \quad (35)$$

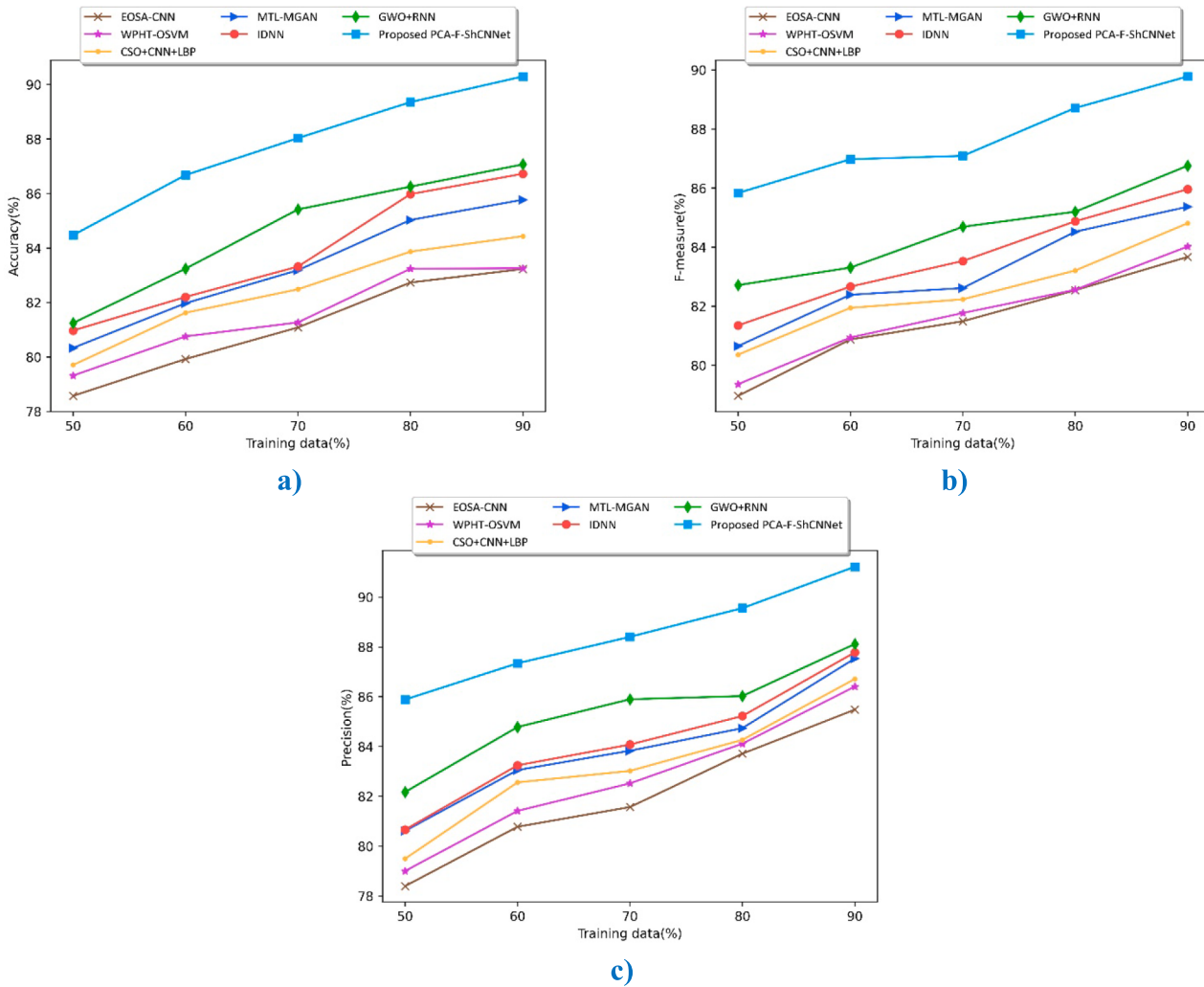


Fig. 9. Comparative estimation based on training data for second-level classification using the developed model, a) accuracy, b) F-measure, c) Precision.

Here, uu specifies the indexes of image coordination, the binary indicator is specified as K , $*$ implies the convolution operation, B indicates the Kernal function and $K_{uu} = 0$ specifies unknown pixel values and pixel to process is given as $K_{uu} = 1$.

The element-wise splitting between the convolved mask and the convolved image naturally controls the way how the pixel details are propagated over all the regions. This enables the ability to handle interpolation for irregularly-spaced data and makes it possible to translate variants. Moreover, the key element of the Shepard method affected the result of interpolation. Hence, employed a new convolutional layer in the light of the Shepard method, which is called the Shepard interpolation layer.

i) Shepard interpolation layer

The feed-forward pass of the trainable interpolation layer is defined as follows,

$$Q_z^a(Q^{a-1}, K^a) = \sigma \left(\sum_q \frac{T_{zq}^a * Q_q^{a-1}}{T_{zq}^a * K_q^a} + u^a \right) \quad (36)$$

where, the index of layers is given as a , feature maps in the layer a , q in Q_q^{a-1} the index feature map in the layer $a-1$. T_{zq} implies the trainable kernel and Q defines the smooth as well as differentiable function. Wherein, σ specifies the nonlinearity of imposed network and bias term is referred as u , here K^a refers mask and input of present layer then the

attained output from ShCNN model is referred as N_x .

The Shepard interpolation layer takes as input both images or feature maps and masks that specify the areas where interpolation should be applied. Also, the interpolation layer is repeatedly applied to design more complex interpolation functions with multiple layers. Here, the same kernel size is applied to the mask and image.

3.2.7. Severity classification using PSA-F-SHCNNNet model

Severity level classification is a critical step in lung cancer detection and diagnosis, as it helps to determine the appropriate treatment plan for patients with lung cancer. The severity level classification of lung cancer is typically based on the following factors, Tumor size, Tumor location, Nodal involvement, Metastatic status and Histopathological type. The classification of lung cancer severity level is the most essential part that helps to minimize the risk of disease progression and reduce misdiagnosis. Here, the severity level classification of lung cancer is performed by the PCA-F-ShCNNNet model. Here the lung cancer detected image N_x is given to classify the severity level of lung cancer. Also, ShCNNNet is capable of classifying lung cancer severity levels with high accuracy. Hence, the classified severity level of lung cancer is indicated as H_x .

4. Results and discussion

This segment estimates the effectiveness of PCA-F-SHCNNNet in

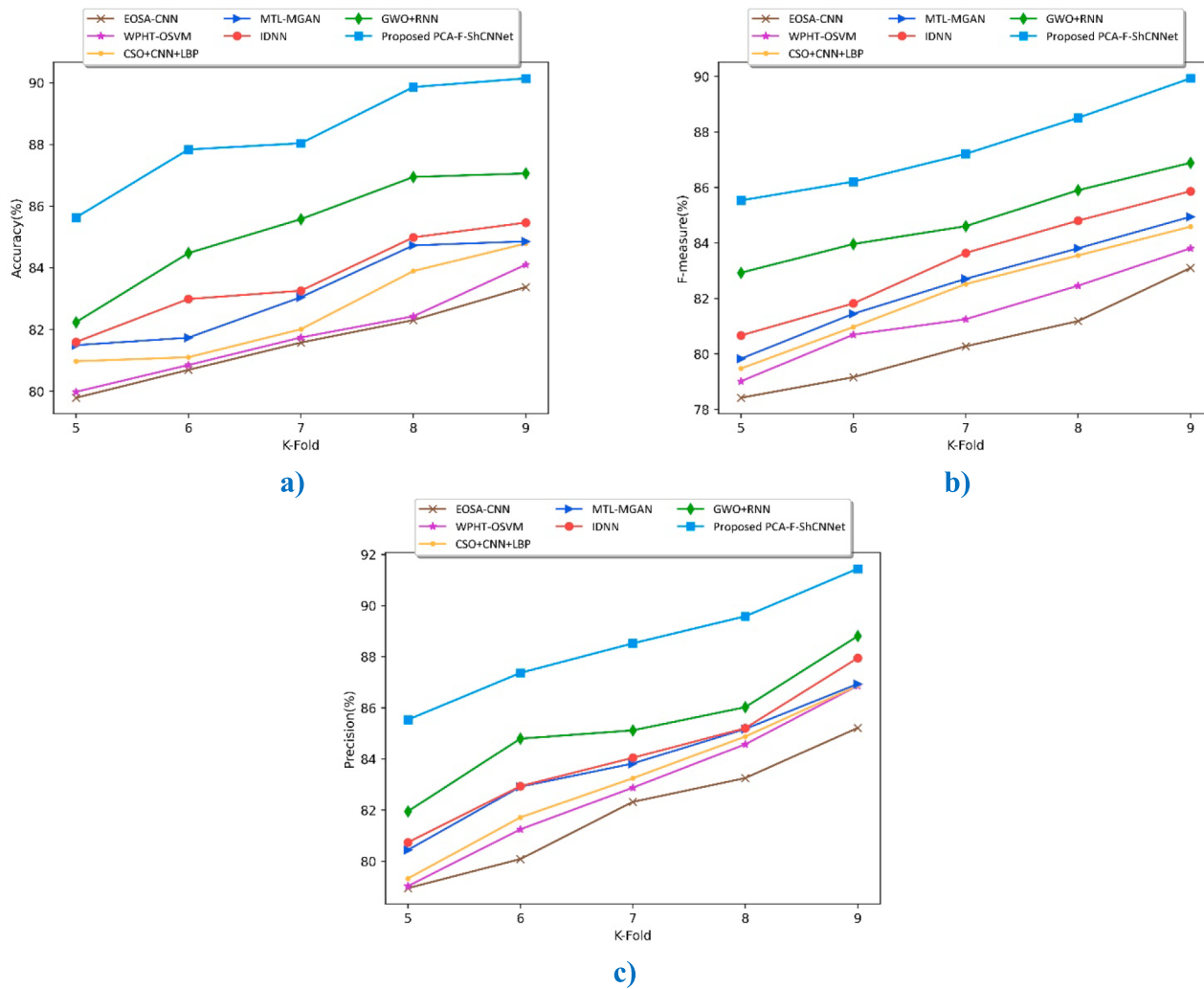


Fig. 10. Comparative valuation based on K-fold for second-level classification using the proposed approach, a) accuracy, b) F-measure, c) Precision.

detecting and classifying lung cancer severity levels classification using CT images. Moreover, the proposed PCA-F-SHCNNNet model is processed using Python, which is evaluated utilizing certain parameters, like F-measure, accuracy, and precision. In this work, the evaluation process considers three important parameters such as epoch, learning rate, and batch size. The value of epoch is 100, learning rate is 0.001, and batch size is 32.

4.1. Experimental results

This section shows the results of the experiment based on the LIDC-IDRI database and IQ-OTH/NCCD – Lung Cancer Dataset.

4.1.1. Image results regarding LIDC-IDRI database

Fig. 5 explains the experimental output of the developed PCA-F-ShCNNNet based on the LIDC-IDRI database to classify and detect lung cancer severity levels using CT images. Here, Fig. 5 a) represents input CT images, Fig. 5 b) specifies pre-processed images, Fig. 5 c) implies segmented CT images, Fig. 5 d) shows nodule-identified lung images and Fig. 5 e) defines the LVP feature extraction for CT lung images.

4.1.2. Image results regarding IQ-OTH/NCCD – lung cancer Dataset

Fig. 6 presents the image results of the PCA-F-ShCNNNet for IQ-OTH/NCCD – Lung Cancer Dataset. Fig. 6 a) displays the original input CT images, Fig. 6 b) shows the pre-processed images, Fig. 6 c) depicts the segmented CT images, Fig. 6 d) represents the lung images with

identified nodules, and Fig. 6 e) displays the LVP feature extraction for the CT lung images.

4.2. Comparative models

The proposed PCA-F-SHCNNNet is compared with different traditional models, like EOSA-CNN [3], CSO + CNN + LBP [7], IDNN [25] and GWO + RNN [15], WPHT-OSVM [26], and MTL-MGAN [5] to show the efficacy.

4.3. Comparative evaluation

The comparative assessment of PCA-F-SHCNNNet is described in this section by adjusting the K-value and training data for two levels of classification based on by LIDC-IDRI database and IQ-OTH/NCCD – Lung Cancer Dataset.

4.3.1. Analysis of PCA-F-ShCNNNet based on first-level classification using LIDC-IDRI database

a) For training data

The estimation of the PCA-F-ShCNNNet is expressed in Fig. 7. Fig. 7 a) presents the valuation of the developed PCA-F-ShCNNNet for accuracy. The accuracy obtained by EOSA-CNN, WPHT-OSVM, CSO + CNN + LBP, MTL-MGAN, IDNN, GWO + RNN and PCA-F-ShCNNNet is 84.44 %, 84.956 %, 85.915 %, 87.078 %, 87.467 %, 88.843 % and 91.567 %, assume 90 % of training data. The F-measure of PCA-F-ShCNNNet is

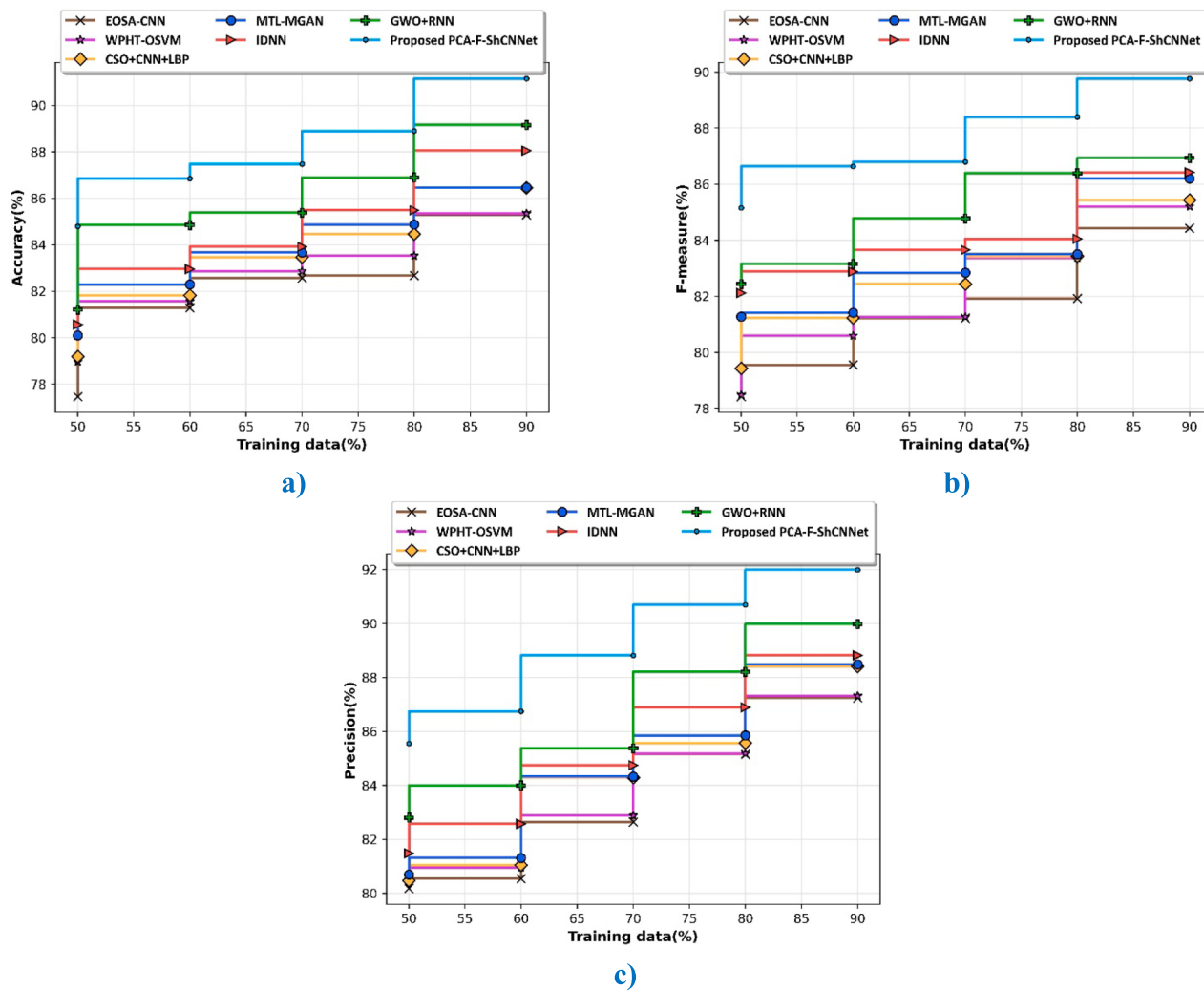


Fig. 11. Comparative analysis for training data based on first-level classification using IQ-OTH/NCCD- Lung Cancer Dataset, a) accuracy, b) F-measure, c) Precision.

evaluated in Fig. 7 b). For 90 % of training data, the F-measure acquired by EOSA-CNN, WPHT-OSVM, CSO + CNN + LBP, MTL-MGAN, IDNN and GWO + RNN is 84.820 %, 84.978 %, 85.397 %, 85.955 %, 86.103 % and 87.388 %, while F-measure of PCA-F-ShCNNet is 90.522 %. The precision of PCA-F-ShCNNet is evaluated in Fig. 7 c). Precision acquired by EOSA-CNN, WPHT-OSVM, CSO + CNN + LBP, MTL-MGAN, IDNN and GWO + RNN is 86.671 %, 86.844 %, 87.781 %, 87.868 %, 88.100 % and 89.895 %, while the precision of PCA-F-ShCNNet is 92.511 %.

b) Using K-fold

The evaluation of the developed PCA-F-ShCNNet by adjusting the K-fold is expressed in Fig. 8. Fig. 8 a) specifies the evaluation of the developed PCA-F-ShCNNet for accuracy. The accuracy acquired by EOSA-CNN, WPHT-OSVM, CSO + CNN + LBP, MTL-MGAN, IDNN, GWO + RNN and proposed PCA-F-ShCNNet is 84.849 %, 85.678 %, 86.969 %, 87.125 %, 87.224 %, 88.423 % and 91.566 %, while K-fold = 9. The F-measure of PCA-F-ShCNNet is evaluated in Fig. 8 b). For the K-fold = 9, the F-measure obtained by EOSA-CNN, WPHT-OSVM, CSO + CNN + LBP, MTL-MGAN, IDNN and GWO + RNN is 84.282 %, 84.408 %, 85.522 %, 86.280 %, 86.558 % and 87.548 %, while F-measure of PCA-F-ShCNNet is 90.490 %. The precision of PCA-F-ShCNNet is presented in Fig. 8 c). When consider the k-fold is 9, the Precision acquired by EOSA-CNN, WPHT-OSVM, CSO + CNN + LBP, MTL-MGAN, IDNN and GWO + RNN is 86.801 %, 87.788 %, 87.876 %, 88.184 %, 88.732 % and 89.831 %, while precision of PCA-F-ShCNNet is 92.598 %.

4.3.2. Comparative estimation of PCA-F-ShCNNet for second-level classification using LIDC-IDRI database

a) Regarding training data

Fig. 9 specifies the comparative evaluation of the devised model by adjusting training data. Fig. 9 a) explains the analysis of the developed PCA-F-ShCNNet for accuracy. Here, the accuracy acquired using EOSA-CNN, WPHT-OSVM, CSO + CNN + LBP, MTL-MGAN, IDNN, GWO + RNN and PCA-F-ShCNNet is 83.229 %, 83.255 %, 84.436 %, 85.775 %, 86.725 %, 87.069 % and 90.296 %, while assuming the training data is 90 %. The F-measure of PCA-F-ShCNNet is evaluated in Fig. 9 b). Considering 90 % of training data, the F-measure acquired by EOSA-CNN, WPHT-OSVM, CSO + CNN + LBP, MTL-MGAN, IDNN and GWO + RNN is 83.670 %, 84.022 %, 84.810 %, 85.369 %, 85.963 % and 86.757 %, while F-measure of PCA-F-ShCNNet is 89.781 %. The precision of PCA-F-ShCNNet is evaluated in Fig. 9 c). Precision acquired by EOSA-CNN, WPHT-OSVM, CSO + CNN + LBP, MTL-MGAN, IDNN and GWO + RNN is 85.481 %, 86.408 %, 86.712 %, 87.534 %, 87.780 % and 88.117 %, while precision of PCA-F-ShCNNet is 91.218 %, for 90 % of training data.

b) Using K-fold

The comparative evaluation of the developed PCA-F-ShCNNet model by changing the K-fold value is specified in Fig. 10. Fig. 10 a) illustrates the evaluation outcome for the accuracy of the developed PCA-F-ShCNNet model. Then, the accuracy obtained by EOSA-CNN, WPHT-OSVM, CSO + CNN + LBP, MTL-MGAN, IDNN, GWO + RNN and PCA-F-ShCNNet is 83.380 %, 84.104 %, 84.793 %, 84.860 %, 85.468 %,

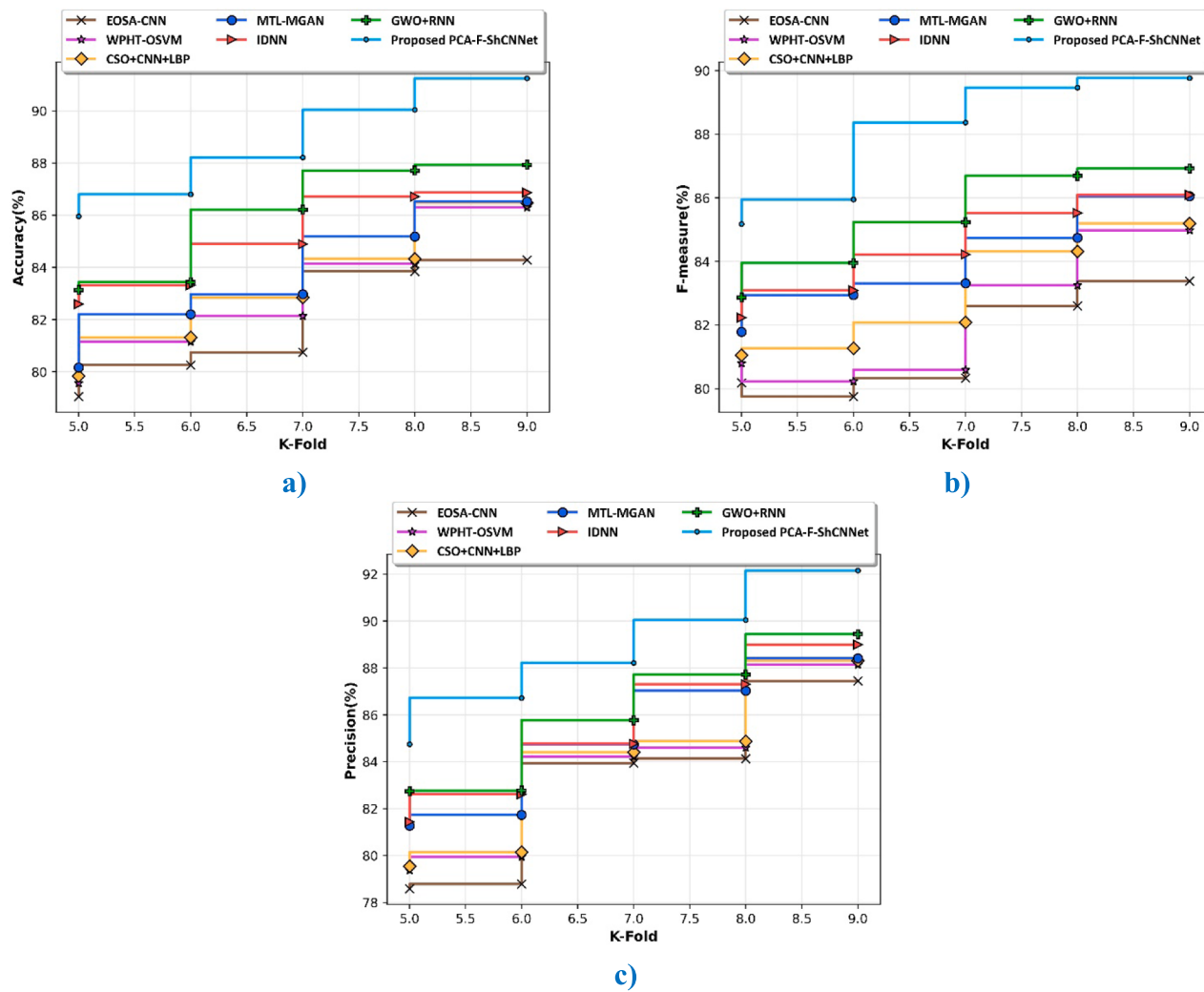


Fig. 12. Comparative estimation regarding K-fold for first-level classification using IQ-OTH/NCCD- Lung Cancer Dataset, a) accuracy, b) F-measure, c) Precision.

87.061 % and 90.143 %, by assuming K-fold = 9. The F-measure of PCA-F-ShCNNet is specified in Fig. 10 b). F-measure acquired by EOSA-CNN, WPHT-OSVM, CSO + CNN + LBP, MTL-MGAN, IDNN and GWO + RNN is 83.100 %, 83.808 %, 84.588 %, 84.943 %, 85.866 % and 86.888 %, while F-measure of PCA-F-ShCNNet is 89.931 % when the k-fold is 9. The precision of PCA-F-ShCNNet is implied in Fig. 10 c). For the k-fold is 9, the Precision attained by EOSA-CNN is 85.219 %, WPHT-OSVM is 86.867 %, CSO + CNN + LBP is 86.868 %, MTL-MGAN is 86.939 %, IDNN as 87.950 % and GWO + RNN as 88.810 %, whereas precision obtained by PCA-F-ShCNNet is 91.443 %.

4.3.3. Analysis of PCA-F-ShCNNet based on first-level classification using IQ-OTH/NCCD – lung cancer Dataset

a) Regarding training data

Fig. 11 presents a comparative evaluation of the PCA-F-ShCNNet methodology based on first-level classification using IQ-OTH/NCCD – Lung Cancer Dataset. In Fig. 11 (a), the accuracy valuation of the PCA-F-ShCNNet is exhibited. Assume 90 % of training data, the accuracy attained the values of 85.280 % for EOSA-CNN, 85.342 % for WPHT-OSVM, 86.446 % for CSO + CNN + LBP, 86.464 % for MTL-MGAN, 88.049 % for IDNN, 89.150 % for GWO + RNN, and 91.150 % for the proposed PCA-F-ShCNNet. Fig. 11 (b) illustrates the analysis of the F-measure of PCA-F-ShCNNet by adjusting the training data. Consider 90 % of training data, then PCA-F-ShCNNet achieved an F-measure of 89.768 %, and the existing techniques, like EOSA-CNN acquired 84.432 %, WPHT-OSVM recorded 85.205 %, CSO + CNN + LBP achieved

85.430 %, MTL-MGAN reached 86.201 %, IDNN gained 86.416 %, and GWO + RNN achieved 86.936 %. The valuation of PCA-F-ShCNNet for Precision is detailed in Fig. 11 (c). For the training data is 90 %, the Precision values attained 87.243 % for EOSA-CNN, 87.317 % for WPHT-OSVM, 88.409 % for CSO + CNN + LBP, 88.480 % for MTL-MGAN, 88.818 % for IDNN, 89.981 % for GWO + RNN and 91.981 % for devised PCA-F-ShCNNet.

b) For K-fold

Fig. 12 represents the evaluation of the devised PCA-F-ShCNNet approach based on first-level classification by varying the K-fold. The accuracy evaluation of PCA-F-ShCNNet is illustrated in Fig. 12 (a). Consider the K-fold = 9, the developed PCA-F-ShCNNet recorded an accuracy of 91.248, while other existing models, like EOSA-CNN, WPHT-OSVM, CSO + CNN + LBP, MTL-MGAN, IDNN, and GWO + RNN acquired the accuracy of 84.284 %, 86.297 %, 86.480 %, 86.529 %, 86.873 %, and 87.937 %. The F-measure valuation of PCA-F-ShCNNet by adjusting the k-fold is demonstrated in Fig. 12 (b). When the K-fold is 9, the PCA-F-ShCNNet achieved a F-measure of 89.760 %, while different methods, like EOSA-CNN attained 83.385 %, WPHT-OSVM acquired 84.985 %, CSO + CNN + LBP reached 85.194 %, MTL-MGAN recorded 86.054 %, IDNN gained 86.098 %, and GWO + RNN acquired 86.922 %. Fig. 12 (c) exhibits an estimation of the precision for the developed PCA-F-ShCNNet method. Considering the k-fold is 9, then the PCA-F-ShCNNet reaches a precision of 92.160 %, while the traditional models, like EOSA-CNN, WPHT-OSVM, CSO + CNN + LBP, MTL-MGAN, IDNN, and GWO + RNN reach a precision of 87.453 %, 88.137

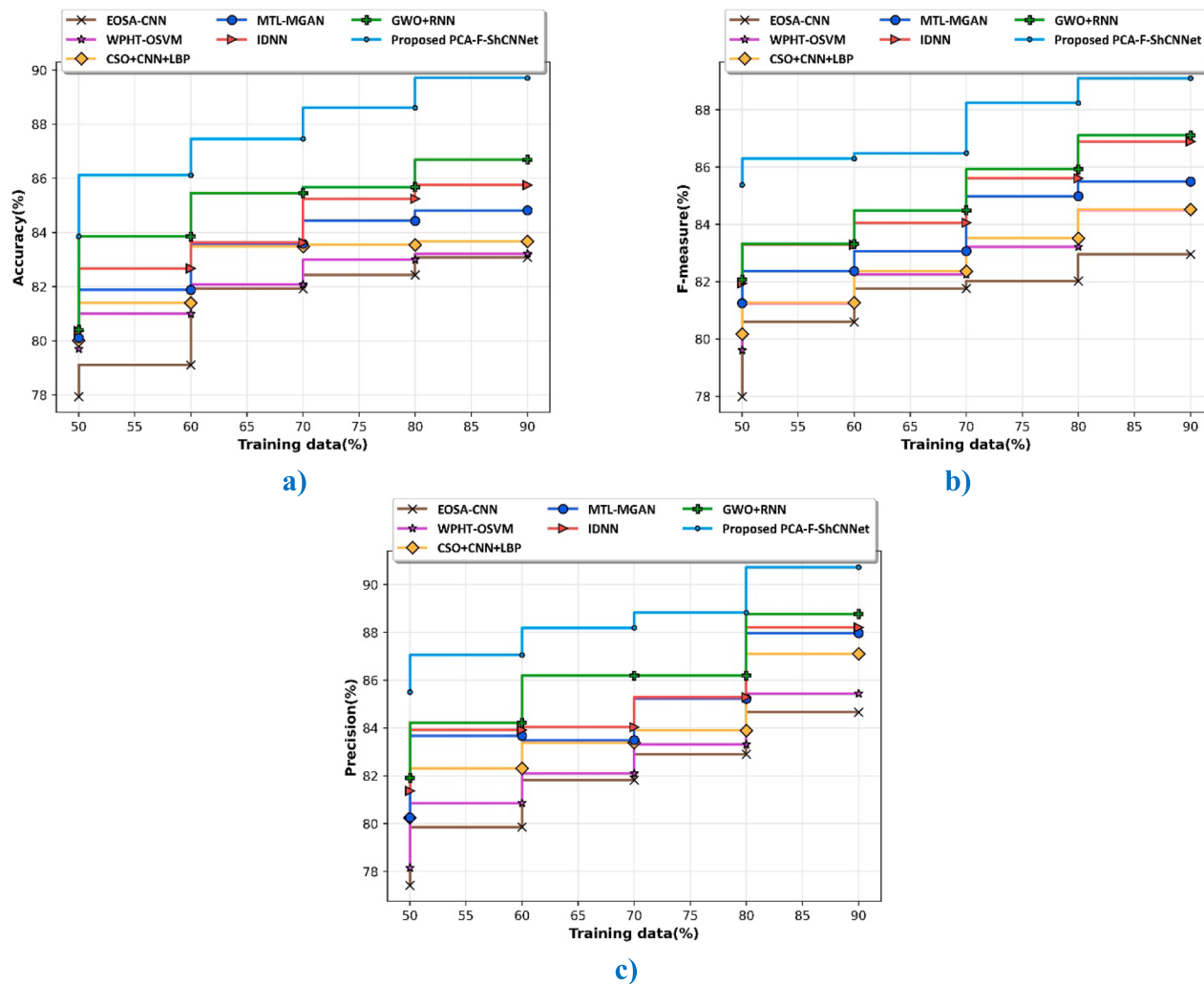


Fig. 13. Comparative estimation based on training data for second-level classification utilizing IQ-OTH/NCCD- Lung Cancer Dataset, a) accuracy, b) F-measure, c) Precision.

%, 88.310 %, 88.411 %, 88.998 %, and 89.446 %.

4.3.4. Analysis of PCA-F-ShCNNet for second-level classification using IQ-OTH/NCCD – lung cancer Dataset

a) Concerning training data

Fig. 13 presents the examination of the PCA-F-ShCNNet based on second-level classification using IQ-OTH/NCCD – Lung Cancer Dataset. Fig. 13 a) illustrates the evaluation of accuracy by adjusting the training data. By considering the training data is 90 %, the accuracy value of EOSA-CNN is 83.077 %, WPHT-OSVM is 83.216 %, CSO + CNN + LBP is 83.665 %, MTL-MGAN is 84.815 %, IDNN is 85.754 %, GWO + RNN is 86.693 %, and proposed PCA-F-ShCNNet is 89.701 %. Fig. 13 b) shows the evaluation for the F-measure. If 90 % of training data, the F-measure value of EOSA-CNN is 82.958 %, WPHT-OSVM is 84.496 %, CSO + CNN + LBP is 84.523 %, MTL-MGAN is 85.493 %, IDNN is 86.899 %, GWO + RNN is 87.104 %, and proposed PCA-F-ShCNNet is 89.104 %. Fig. 13 c) signifies the assessment of precision by increasing the training data. When considering 90 % of training data, the conventional models such as EOSA-CNN, WPHT-OSVM, CSO + CNN + LBP, MTL-MGAN, IDNN, and GWO + RNN attained the precision of 84.657 %, 85.446 %, 87.103 %, 87.974 %, 88.211 %, and 88.772 % and then the proposed PCA-F-ShCNNet model gained the precision of 90.730 %.

b) Concerning K-fold

Fig. 14 signifies the assessment of the devised approach based on the IQ-OTH/NCCD – Lung Cancer Dataset concerning K-fold. Fig. 14 a)

illustrates the valuation of accuracy by adjusting K-fold. When considering the k-fold is 9, the value of accuracy is 83.691 % for EOSA-CNN, 84.582 % for WPHT-OSVM, 84.869 % for CSO + CNN + LBP, 85.184 % for MTL-MGAN, 85.465 % for IDNN, 87.458 % for GWO + RNN, and 89.811 % for proposed PCA-F-ShCNNet. Fig. 14 b) depicts the analysis of the F-measure concerning K-fold. By assuming the k-fold as 9, the f-measure gained by the traditional models like EOSA-CNN is 82.734 %, WPHT-OSVM is 84.355 %, CSO + CNN + LBP is 85.056 %, MTL-MGAN is 85.083 %, IDNN is 85.565 %, and GWO + RNN is 87.325 %. Moreover, the proposed PCA-F-ShCNNet achieved the F-measure is 89.325 %. Fig. 14 c) indicates the valuation of precision by varying K-fold. While considering the k-fold as 9, the values of precision are 86.036 % for EOSA-CNN, 87.272 % for WPHT-OSVM, 87.393 % for CSO + CNN + LBP, 87.397 % for MTL-MGAN, 88.363 % for IDNN, 88.564 % for GWO + RNN and 90.675 % for proposed PCA-F-ShCNNet.

4.4. Comparative discussion

This part refers to the comparative discussion of developed PCA-F-ShCNNet and existing methods, like EOSA-CNN, WPHT-OSVM, CSO + CNN + LBP, MTL-MGAN, IDNN and GWO + RNN for K-fold and training data using LIDC-IDRI database and IQ-OTH/NCCD- Lung Cancer Dataset. The comparative discussion of PCA-F-ShCNNet concerning evaluation metrics is explained in Table 1. The traditional model attained an accuracy of 84.849 %, 85.678 %, 86.969 %, 87.125 %,

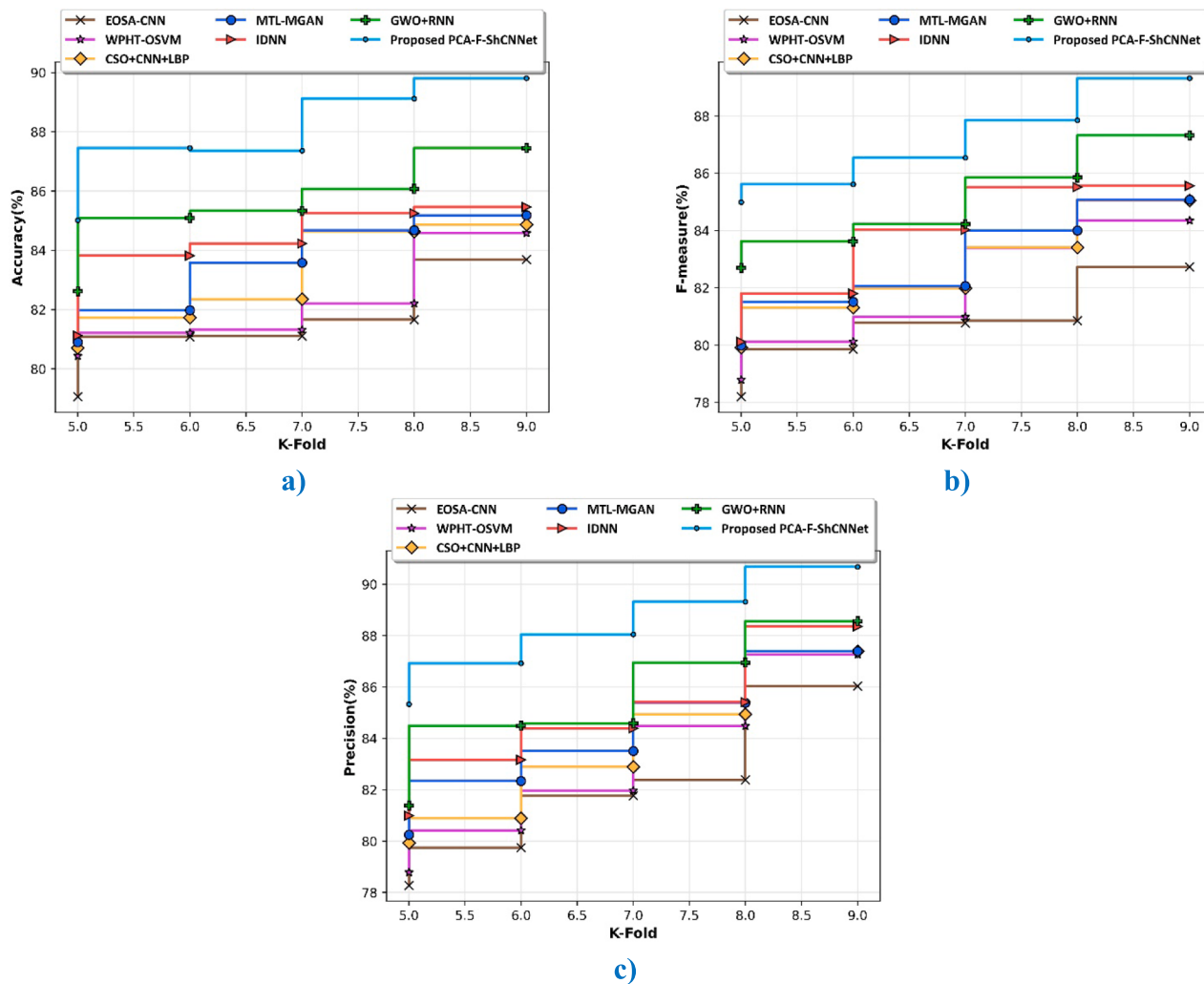


Fig. 14. Comparative evaluation for K-fold based on second-level classification using IQ-OTH/NCCD- Lung Cancer Dataset, a) accuracy, b) F-measure, c) Precision.

87.224 % and 88.423 %, whereas the highest accuracy obtained by the developed model is 91.566 %. Therefore, the model is capable of providing more insights into features that are essential to classify and detect the severity level of lung cancer and enhance interpretability. F-measure acquired by EOSA-CNN is 84.282 %, WPHT-OSVM is 84.408 %, CSO + CNN + LBP is 85.522 %, MTL-MGAN is 86.280 %, IDNN is 86.558 % and GWO + RNN is 87.548 %, while F-measure value obtained by PCA-F-ShCNNNet is 90.490 %, when K-fold = 9. The precision obtained by EOSA-CNN, WPHT-OSVM, CSO + CNN + LBP, MTL-MGAN, IDNN and GWO + RNN is 86.801 %, 87.788 %, 87.876 %, 88.184 %, 88.732 % and 89.831 %, while precision acquired by proposed PCA-F-ShCNN model as 92.598 %. This clearly shows the developed model effectively minimized false positive cases and improved the outcome of patients.

Research Limitations

The drawbacks of this research are explained below:

- In this research, the CT images can vary greatly between patients due to differences in anatomy, disease stage, and imaging protocols, which makes it difficult for models to generalize across different populations.
- Accurate labeling of medical images requires expertise, and the process is time-consuming and subjective. Mislabeling or inconsistencies in annotations can degrade the performance of the proposed model, especially when detecting small or early-stage nodules.

- The devised model typically requires significant computational resources for both inference and training, which makes it difficult to deploy them in resource-constrained clinical settings, particularly in low-resource areas.

5. Conclusion

This work presents an innovative approach, PCA-F-ShCNNNet, combining PCANet and ShCNN to classify its severity and detect lung cancer. The process includes pre-processing with AWF to reduce noise, and then the segmentation using U-Net, and nodule identification through a grid-based approach. The effectiveness of the developed PCA-F-ShCNNNet method is evaluated by metrics, such as accuracy, F-measure and precision, which have the highest values of 91.566 %, 90.490 % and 92.598 %. The advantages of this research are that the proposed model enhances feature extraction and classification, improving the accuracy of lung cancer detection from CT images, by combining PCANet and ShCNN. Also, the integration of U-Net for lung lobe segmentation provides precise and robust segmentation, which is crucial for accurate nodule detection and diagnosis. Moreover, the grid-based approach for nodule identification ensures thorough and systematic detection of potential lung nodules, reducing the chances of missing critical information. The model not only detects lung cancer but also classifies the severity level, providing additional valuable information for clinical decision-making. In future, the model will be extended by implementing the Federated Learning (FL) technique to secure and analyze the

Table 1
Comparative discussion.

Setups	Metrics	EOSA-CNN	WPHT-OSVM	CSO + CNN + LBP	MTL-MGAN	IDNN	GWO + RNN	Proposed PCA-F-ShCNNNet
LIDC-IDRI database (First level)								
Training Data = 90 %	Accuracy (%)	84.444	84.956	85.915	87.078	87.467	88.843	91.567
	F-measure (%)	84.820	84.978	85.397	85.955	86.103	87.388	90.522
	Precision (%)	86.671	86.844	87.781	87.868	88.100	89.895	92.511
K-Fold = 9	Accuracy (%)	84.849	85.678	86.969	87.125	87.224	88.423	91.566
	F-measure (%)	84.282	84.408	85.522	86.280	86.558	87.548	90.490
	Precision (%)	86.801	87.788	87.876	88.184	88.732	89.831	92.598
LIDC-IDRI database (Second level)								
Training Data = 90 %	Accuracy (%)	83.229	83.255	84.436	85.775	86.725	87.069	90.296
	F-measure (%)	83.670	84.022	84.810	85.369	85.963	86.757	89.781
	Precision (%)	85.481	86.408	86.712	87.534	87.780	88.117	91.218
K-Fold = 9	Accuracy (%)	83.380	84.104	84.793	84.860	85.468	87.061	90.143
	F-measure (%)	83.100	83.808	84.588	84.943	85.866	86.888	89.931
	Precision (%)	85.219	86.867	86.868	86.939	87.950	88.810	91.443
IQ-OTH/NCCD – Lung Cancer Dataset (First level)								
Training Data = 90 %	Accuracy (%)	85.280	85.342	86.446	86.464	88.049	89.150	91.150
	F-measure (%)	84.432	85.205	85.430	86.201	86.416	86.936	89.768
	Precision (%)	87.243	87.317	88.409	88.480	88.818	89.981	91.981
K-Fold = 9	Accuracy (%)	84.284	86.297	86.480	86.529	86.873	87.937	91.248
	F-measure (%)	83.385	84.985	85.194	86.054	86.098	86.922	89.760
	Precision (%)	87.453	88.137	88.310	88.411	88.998	89.446	92.160
IQ-OTH/NCCD – Lung Cancer Dataset (Second level)								
Training Data = 90 %	Accuracy (%)	83.077	83.216	83.665	84.815	85.754	86.693	89.701
	F-measure (%)	82.958	84.496	84.523	85.493	86.899	87.104	89.104
	Precision (%)	84.657	85.446	87.103	87.974	88.211	88.772	90.730
K-Fold = 9	Accuracy (%)	83.691	84.582	84.869	85.184	85.465	87.458	89.811
	F-measure (%)	82.734	84.355	85.056	85.083	85.565	87.325	89.325
	Precision (%)	86.036	87.272	87.393	87.397	88.363	88.564	90.675

information about the patients. Moreover, future research will aim to integrate techniques like GAN to generate synthetic data, particularly for rare cases such as small or atypical lung nodules, helping to balance datasets and improve model performance on underrepresented classes.

CRediT authorship contribution statement

SK Altaf Hussain Basha: Visualization. **Pravin R. Kshirsagar:** Visualization, Project administration, Data curation. **P Srinivasa Rao:**

Appendix

Architecture of U-Net.

The U-Net [30] is divided into two parts, first, the contracting path is used for the typical CNN framework. In the contracting path, each block consists of two consecutive 3×3 convolution layers followed by a ReLU activation unit and a max-pooling layer. This configuration is repeated multiple times. The innovation of U-Net, however, lies in the second part, known as the expansive path. In this phase, each stage upscales the feature maps using a 2×2 up-convolution. Hence, the network energy function is given as,

$$M = \sum r(d') \log(\psi_J(d')) \quad (A1)$$

where pixel-wise softmax function ψ_J is applied in the final feature map that is denoted as,

$$\psi_J \exp(k'_J(d')) / \sum_{jj=1}^J \exp(k'_J(d')) \quad (A2)$$

Fig. A1 shows the general outline for U-Net. Therefore, k'_J specifies activation in the channel J and the obtained output from U-Net is denoted as W_x .

Software, Formal analysis. **Tan Kuan Tak:** Writing – review & editing. **B. Sivaneasan:** Visualization.

Declaration of competing interest

The authors declare that they have no known competing financial interests or personal relationships that could have appeared to influence the work reported in this paper.

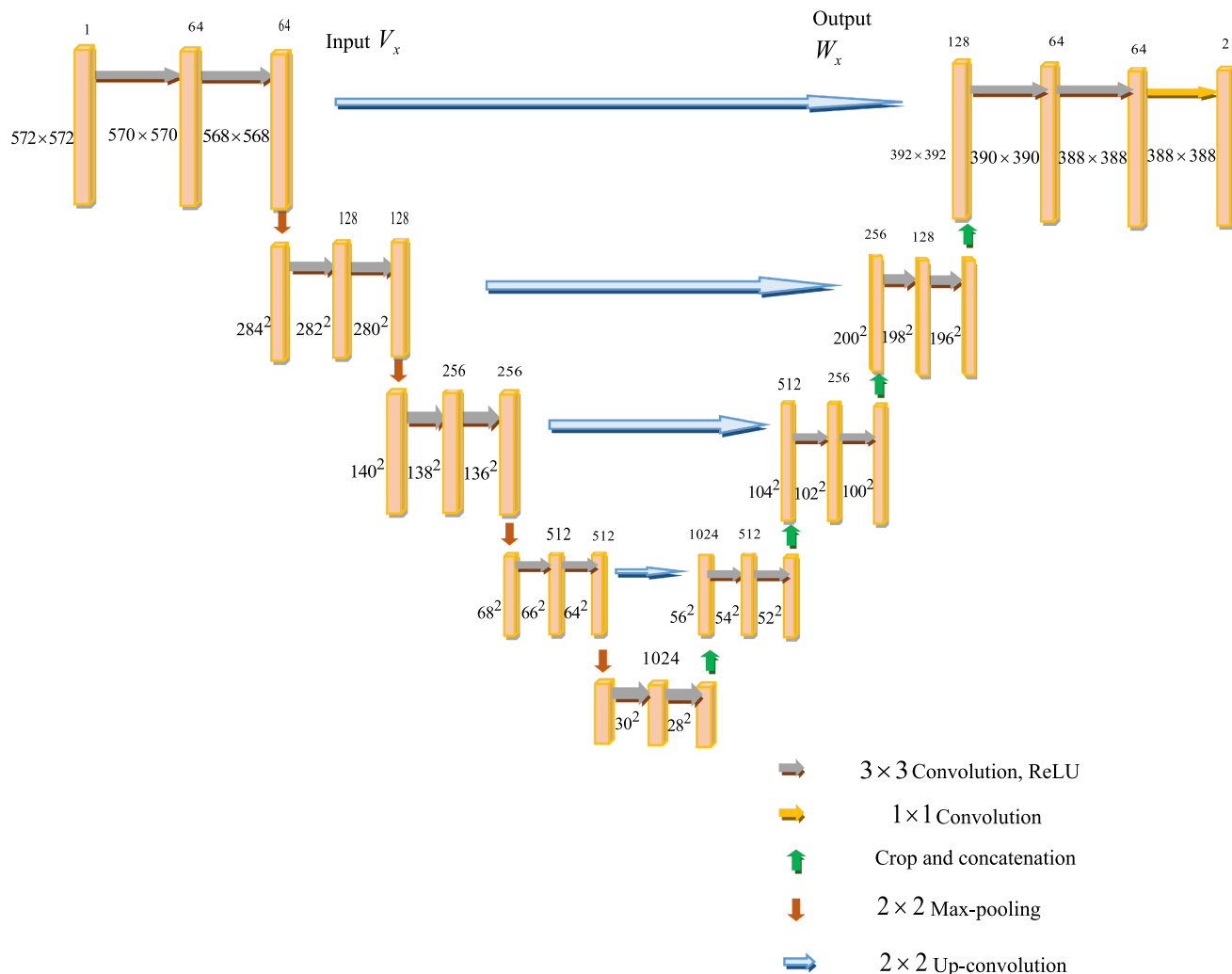


Fig. A1. General outline for U-Net used for the segmentation of lung lobe

Performance assessment

This section describes the performance assessment based on two datasets as LIDC-IDRI database and IQ-OTH/NCCD – Lung Cancer Dataset for two levels of classification by adjusting the K-fold and training data.

Performance assessment based on first-level classification using LIDC-IDRI database.

a) Using training data

Table A1 shows the performance evaluation of the proposed PCA-F-ShCNNet model for first-level classification concerning the training data. The accuracy improves consistently as both the number of epochs and the size of the training data increase. For example, with 50 % of training data, the accuracy increases from 79.636 % at Epoch 20 to 85.047 % at Epoch 100. The F-measure also shows steady growth across both epochs and training sizes, indicating that the model is increasingly balancing precision and recall. At Epoch 100, the F-measure reaches the value of 85.406 % for 50 % of training data and 90.587 % for 90 % of training data, reflecting strong classification performance. Precision demonstrates a clear upward trend across all epochs and training data sizes. At Epoch 100, for 50 % of the training data, the precision value is 86.118 %, while for the training data is 90 %, it peaks at 92.539 %.

Table A1

Performance estimation of PCA-F-ShCNNet concerning first-level classification.

Epoch/ Training data (%)	Epoch 20	Epoch 40	Epoch 60	Epoch 80	Epoch 100
Accuracy (%)					
50	79.636	83.032	83.032	83.295	85.047
60	83.027	83.699	84.007	85.579	87.645
70	84.406	85.034	86.422	86.613	88.982
80	84.825	85.580	87.113	87.215	89.125
90	87.298	87.469	88.389	89.319	91.679
F-measure (%)					
50	78.191	79.369	81.115	82.503	85.406
60	78.857	80.895	81.775	83.959	86.081
70	80.030	81.601	82.781	85.471	87.619
80	80.895	85.260	86.857	86.857	88.942
90	85.654	86.242	87.335	88.522	90.587
Precision (%)					
50	79.954	81.892	83.158	83.933	86.118
60	79.958	82.774	85.086	85.091	87.211
70	83.748	84.122	85.736	87.068	89.214
80	85.017	85.618	87.068	88.969	91.147
90	86.467	88.308	88.573	90.511	92.539

b) Concerning K-fold

The performance evaluation of the PCA-F-ShCNNet model with K-fold and more training epochs is demonstrated in **Table A2**. Here, the proposed achieved the highest accuracy of 91.691 % at Epoch 100, for 9 as k-fold. The F-measure shows consistent enhancement across both the epochs and K-values. At Epoch 100, the F-measure ranges from 85.621 % for 5-fold to 90.632 for 9-fold, indicating a better balance between precision and recall as the model is trained on more folds. Precision follows the same positive trend, with higher K-fold values contributing to more precise classification. At Epoch 100, the precision increases from 85.559 % for 5-fold to 92.636 % for 9-fold.

Table A2

Performance estimation of PCA-F-ShCNNet based on first-level classification.

Epoch/ K-fold	Epoch 20	Epoch 40	Epoch 60	Epoch 80	Epoch 100
Accuracy (%)					
5	79.138	79.936	80.972	84.585	86.724
6	79.259	80.428	84.585	85.560	87.615
7	81.975	84.352	85.122	86.209	88.819
8	84.522	84.755	88.432	88.432	90.444
9	85.221	87.425	89.520	89.566	91.691
F-measure (%)					
5	77.873	78.071	78.388	79.554	85.621
6	79.249	79.701	79.847	80.782	86.429
7	79.980	80.415	80.603	82.006	88.013
8	84.306	86.003	87.244	87.776	89.844
9	87.347	88.025	88.490	88.490	90.632
Precision (%)					
5	77.629	79.797	80.657	83.547	85.559
6	79.803	82.291	83.658	84.997	87.087
7	82.740	83.964	84.575	85.719	88.758
8	83.150	84.406	86.627	88.717	90.894
9	86.706	87.475	88.598	90.598	92.636

Performance assessment based on second-level classification using LIDC-IDRI database.**a) For training data**

Table A3 highlights the performance analysis of the PCA-F-ShCNNet model's second-level classification by varying the number of epochs and training data. Here, the maximum accuracy of 90.367 % is recorded at Epoch 100 with training data of 90 %, indicating that the highest training databases and more epochs enhance the model's performance. At Epoch 100, the F-measure ranges from 85.872 % for 50 % of training data to 89.910 % for 90 % of training data. Precision follows a similar upward trend. For instance, at Epoch 100, precision increases from the value of 85.972 % for 50 % of training data to 91.336 % for 90 % of training data.

Table A3

Performance analysis of PCA-F-ShCNNet based on second-level classification.

Epoch/ Training data (%)	Epoch 20	Epoch 40	Epoch 60	Epoch 80	Epoch 100
Accuracy (%)					
50	77.553	78.697	80.149	82.475	84.536
60	79.296	79.485	81.949	83.035	86.860
70	81.338	82.874	83.947	84.677	88.165
80	82.700	84.080	84.677	85.322	89.383
90	84.432	84.682	85.020	88.296	90.367
F-measure (%)					
50	78.178	78.565	78.941	83.212	85.872
60	79.303	80.551	82.799	85.094	86.103
70	81.361	82.445	83.430	85.095	87.123
80	82.237	82.486	84.977	86.605	88.768
90	84.205	84.343	87.781	87.781	89.910
Precision (%)					
50	78.403	81.062	82.048	83.886	85.972
60	80.753	83.886	83.886	85.339	87.477
70	82.658	84.334	85.342	86.017	88.521
80	83.616	85.239	86.406	86.406	89.587
90	85.219	86.889	87.568	88.620	91.336

b) Utilizing K-fold

Table A4 shows the evaluation of the performance of the PCA-F-ShCNNet for second-level classification across varying epochs and K-fold. The developed model performs best with 9-fold cross-validation, where it achieves the highest accuracy of 90.336 % at Epoch 100. If the k-fold is 9, the devised scheme measured the maximum f-measure of 90.050 % at epoch 100. Moreover, the highest precision value of the devised scheme is 91.461 % for 9-fold, highlighting the model's improving ability to correctly classify positive instances as the number of training folds increases.

Table A4

Performance evaluation of PCA-F-ShCNNet for second-level classification.

Epoch/ K-fold	Epoch 20	Epoch 40	Epoch 60	Epoch 80	Epoch 100
Accuracy (%)					
5	78.407	80.196	81.684	83.634	85.711
6	79.948	82.155	83.302	85.881	87.918
7	80.982	83.568	84.571	86.040	88.171
8	81.825	85.832	87.440	87.861	89.866
9	83.339	86.827	87.593	88.143	90.336
F-measure (%)					
5	77.277	79.752	81.905	82.601	85.559
6	78.464	80.004	83.535	83.535	86.310
7	79.907	81.696	83.714	84.208	87.396
8	80.392	82.966	84.873	86.237	88.622
9	82.115	83.646	85.011	87.326	90.050
Precision (%)					
5	77.313	81.385	81.717	83.178	85.666
6	80.808	82.310	82.627	85.368	87.487
7	82.052	83.808	84.572	86.527	88.670
8	82.947	85.927	86.458	87.583	89.587
9	84.751	86.941	88.214	88.662	91.461

Performance assessment based on first-level classification using IQ-OTH/NCCD – Lung Cancer Dataset.**a) Utilizing training data**

The performance estimation of the PCA-F-ShCNNet based on first-level classification is depicted in **Table A5**. Here, the evaluation is based on three key metrics includes: Accuracy, F-measure, and Precision. The devised model achieves its highest accuracy of 91.258 % at Epoch 100 with 90 % training data, indicating that larger datasets and more epochs contribute significantly to better performance. Subsequently, at Epoch 100, the developed approach gained the maximum F-measure of 89.947 % for 90 % of training data, indicating an enhanced ability of the model to balance precision and recall as training data size and epochs increase. Moreover, the PCA-F-ShCNNet achieved the maximum precision of 92.117 % for 90 % of the training samples. This reflects the growing capability of the model to make accurate positive classifications as it is trained on more data and for more epochs.

Table A5

Performance analysis of PCA-F-ShCNNet based on first-level classification.

Epoch/ Training data (%)	Epoch 20	Epoch 40	Epoch 60	Epoch 80	Epoch 100
Accuracy (%)					
50	76.021	77.512	79.236	82.789	84.895
60	80.860	81.797	83.691	84.264	86.908
70	81.496	83.561	84.655	84.713	87.637
80	84.212	84.357	86.894	86.894	89.075
90	87.814	88.977	89.150	89.150	91.258
F-measure (%)					
50	76.994	78.763	79.917	81.230	85.170
60	79.114	79.472	83.156	83.156	86.803
70	82.366	83.334	84.796	85.058	87.965
80	84.503	85.758	86.394	86.522	88.465
90	84.531	87.308	87.768	87.768	89.947
Precision (%)					
50	79.968	80.854	82.718	83.547	85.630
60	80.533	82.387	83.547	83.962	86.775
70	82.345	84.156	84.740	84.919	88.919
80	83.184	84.162	85.557	88.142	90.784
90	85.558	86.494	86.546	89.676	92.117

b) For K-fold

Table A6 illustrates the evaluation of the PCA-F-ShCNNet model's performance for first-level classification across varying epochs and different K-fold values. At epoch 100 with K-fold is 9, the PCA-F-ShCNNet model achieved the maximum accuracy of 91.294 %, f-measure of 89.903 %, and precision of 92.221 %. Moreover, the developed model achieves its best results with 9-fold cross-validation and 100 epochs, demonstrating the importance of both extended training and cross-validation for optimizing model performance.

Table A6

Performance evaluation of PCA-F-ShCNNet for first-level classification.

Epoch/ K-fold	Epoch 20	Epoch 40	Epoch 60	Epoch 80	Epoch 100
Accuracy (%)					
5	77.692	79.347	82.269	83.957	86.091
6	80.901	81.356	83.610	84.800	86.804
7	82.607	83.513	84.432	86.216	88.258
8	83.732	84.193	87.394	88.036	90.117
9	84.304	86.292	88.465	88.698	91.294
F-measure (%)					
5	79.159	81.256	81.689	83.180	85.362
6	79.460	82.005	82.463	83.949	86.019
7	80.935	82.199	82.952	85.369	87.463
8	80.960	83.746	85.334	86.038	88.619
9	83.353	85.053	86.417	87.468	89.903
Precision (%)					
5	78.217	78.448	80.266	83.005	84.926
6	79.472	82.491	82.753	83.351	86.844
7	82.012	82.753	85.172	86.221	88.416
8	83.017	84.013	85.396	87.740	90.058
9	85.798	86.204	88.296	88.893	92.221

Performance assessment based on second-level classification using IQ-OTH/NCCD – Lung Cancer Dataset.**a) Concerning training data**

Table A7 evaluates the PCA-F-ShCNNet model's performance estimation for second-level classification across different epochs by varying training data. Here, the accuracy shows a consistent increase as both the number of training epochs and data size grow. For example, at Epoch 100, accuracy increases from 83.905 % for 50 % training data to 89.725 % for 90 % training data. Moreover, the devised scheme reached the maximum f-measure of 89.115 % and precision of 90.915 %, at epoch 100 with 90 % of training data. The results suggest that larger datasets and longer training durations are crucial for maximizing classification accuracy in second-level tasks.

Table A7

Performance analysis of PCA-F-ShCNNet based on second-level classification.

Epoch/ Training data (%)	Epoch 20	Epoch 40	Epoch 60	Epoch 80	Epoch 100
Accuracy (%)					
50	77.113	77.986	80.555	81.862	83.905
60	77.393	80.177	83.718	84.113	86.289
70	81.291	81.909	84.049	85.459	87.476
80	81.398	81.922	84.982	86.609	88.693
90	83.040	86.259	87.546	87.703	89.725
F-measure (%)					
50	76.316	77.638	81.618	82.154	85.516
60	79.713	80.162	81.702	82.724	86.326
70	80.088	82.743	83.932	84.491	87.584
80	81.103	84.491	84.491	86.235	88.360
90	83.271	85.285	86.104	87.104	89.115
Precision (%)					
50	75.824	77.497	79.661	80.649	85.691
60	78.548	79.431	81.874	85.180	87.115
70	80.273	83.068	85.205	85.922	88.302
80	81.424	83.441	85.784	86.823	89.915
90	83.915	84.721	88.730	88.771	90.915

b) Using K-fold

The performance evaluation of the PCA-F-ShCNNet for second-level classification, considering different epochs and K-fold values is displayed in **Table A8**. The evaluation is based on three key metrics: Accuracy, F-measure, and Precision. At Epoch 100 with 9-fold cross-validation, the model achieved its highest performance, with an accuracy of 89.893 %, F-measure of 89.365 %, and precision of 90.826 %. These results underscore the significant role that both extended training periods and higher K-fold cross-validation play in optimizing the model's performance.

Table A8

Performance evaluation of PCA-F-ShCNNet for second-level classification.

Epoch/ K-fold	Epoch 20	Epoch 40	Epoch 60	Epoch 80	Epoch 100
Accuracy (%)					
5	77.434	80.214	83.011	83.011	85.203
6	79.657	80.653	83.472	85.457	86.470
7	81.254	81.970	84.738	85.306	87.388
8	81.548	82.603	85.457	86.812	88.191
9	81.718	83.054	87.811	87.811	89.893
F-measure (%)					
5	78.790	80.387	81.220	83.275	85.153
6	78.904	80.488	81.630	83.620	85.753
7	80.111	81.266	82.309	84.542	86.584
8	81.629	82.993	82.993	85.854	87.918
9	85.135	86.213	87.325	87.348	89.365
Precision (%)					
5	78.574	79.832	82.582	83.329	85.494
6	79.137	82.338	82.891	84.307	86.989
7	80.453	82.498	83.329	84.923	88.220
8	82.237	83.329	84.554	87.465	89.495
9	84.338	87.783	88.675	88.675	90.826

Data availability

<https://wiki.cancerimagingarchive.net/display/Public/LIDC-IDRI>

References

- [1] Woodman, C., Vundu, G., George, A. and Wilson, C.M., "Applications and strategies in nanodiagnosis and nanotherapy in lung cancer", In Seminars in cancer biology, vol. 69, pp. 349-364, Academic Press, February 2021.
- [2] Sung, H., Ferlay, J., Siegel, R.L., Laversanne, M., Soerjomataram, I., Jemal, A. and Bray, F., "Global cancer statistics 2020: GLOBOCAN estimates of incidence and mortality worldwide for 36 cancers in 185 countries", CA: a cancer journal for clinicians, vol. 71, no. 3, pp.209-249, 2021.
- [3] T.I. Mohamed, O.N. Oyelade, A.E. Ezugwu, Automatic detection and classification of lung cancer CT scans based on deep learning and ebola optimization search algorithm, PLoS One 18 (8) (2023).
- [4] R. Raza, F. Zulfiqar, M.O. Khan, M. Arif, A. Alvi, M.A. Iftikhar, T. Alam, Lung-EffNet: Lung cancer classification using EfficientNet from CT-scan images, Eng. Appl. Artif. Intel. 126 (2023) 106902.
- [5] Y. Luo, C. Chen, J.H. Adamek, D. Crocetti, S.H. Mostofsky, J.B. Ewen, Altered cortical activation associated with mirror overflow driven by non-dominant hand movement in attention-deficit/hyperactivity disorder, Prog. Neuropsychopharmacol. Biol. Psychiatry 112 (2022).
- [6] G. De Nunzio, A. Massafra, R. Cataldo, I. De Mitri, M. Peccarisi, M.E. Fantacci, G. Gargano, E.L. Torres, Approaches to juxta-pleural nodule detection in CT images within the MAGIC-5 Collaboration, Nucl. Instrum. Methods Phys. Res., Sect. A 648 (2011) S103–S106.
- [7] C. Venkatesh, K. Ramana, S.Y. Lakkisetti, S.S. Band, S. Agarwal, A. Mosavi, A neural network and optimization based lung cancer detection system in CT images, Front. Public Health 10 (2022) 769692.
- [8] I. Shafi, S. Din, A. Khan, I.D.L.T. Díez, R.D.J.P. Casanova, K.T. Pifarre, I. Ashraf, An effective method for lung cancer diagnosis from ct scan using deep learning-based support vector network, Cancers 14 (21) (2022) 5457.
- [9] Y. Muhammad, M. Tahir, M. Hayat, K.T. Chong, Early and accurate detection and diagnosis of heart disease using intelligent computational model, Sci. Rep. 10 (1) (2020) 19747.

- [10] Pour, E.S. and Esmaeili, M., "Lung Cancer Detection from CT Scan Images based on Genetic-Independent Recurrent Deep Learning", arXiv preprint arXiv: 2312.03185, 2023.
- [11] Pagadala, P.K., Pinapatruni, S.L., Kumar, C.R., Katakam, S., Peri, L.S.K. and Reddy, D.A., "Enhancing Lung Cancer Detection from Lung CT Scan Using Image Processing and Deep Neural Networks", *Revue d'Intelligence Artificielle*, vol. 37, no. 6, 2023.
- [12] Y. Luo, J. Zhang, C. Wang, X. Zhao, Q. Chang, H. Wang, C. Wang, Discriminating schizophrenia disease progression using a P50 sensory gating task with dense-array EEG, clinical assessments, and cognitive tests, *Expert Rev. Neurother.* 19 (2019).
- [13] T.H. Chan, K. Jia, S. Gao, J. Lu, Z. Zeng, Y. Ma, PCANet: A simple deep learning baseline for image classification? *IEEE Trans. Image Process.* 24 (12) (2015) 5017–5032.
- [14] Y. Xiao, Z. Liu, H. Yin, X. Wang, Y. Zhang, STFormer: A dual-stage transformer model utilizing spatio-temporal graph embedding for multivariate time series forecasting, *J. Intell. Fuzzy Syst.* (2024).
- [15] V.K. Gunjan, N. Singh, F. Shaik, S. Roy, Detection of lung cancer in CT scans using grey wolf optimization algorithm and recurrent neural network, *Heal. Technol.* 12 (6) (2022) 1197–1210.
- [16] V. Suganya, S. Selvi, N. Ashokkumar, S. Prema, An Automated Lion-Butterfly Optimization (LBO) based Stacking Ensemble Learning Classification (SELCL) Model for Lung Cancer Detection, *Iraqi Journal for Computer Science and Mathematics* 4 (3) (2023) 87–100.
- [17] Kwok Tai Chui, Brij B. Gupta, Rutvij H. Jhaveri, Hao Ran Chi, Varsha Arya, Ammar Almomani, and Ali Nauman, "Multiround Transfer Learning and Modified Generative Adversarial Network for Lung Cancer Detection", *International Journal of Intelligent Systems*, 2023.
- [18] S. Wankhade, S. Vigneshwari, A novel hybrid deep learning method for early detection of lung cancer using neural networks, *Healthcare Anal.* 3 (2023) 100195.
- [19] Tiwari, A., Hannan, S.A., Pinnamaneni, R., Al-Ansari, A.R.M., El-Ebary, Y.A.B., Prema, S., Manikandan, R. and Vidalón, J.L.J., "Optimized Ensemble of Hybrid RNN-GAN Models for Accurate and Automated Lung Tumour Detection from CT Images", *International Journal of Advanced Computer Science and Applications*, vol. 14, no. 7, 2023.
- [20] Y. Xiao, H. Yin, Y. Zhang, H. Qi, Y. Zhang, Z. Liu, A dual-stage attention-based Conv-LSTM network for spatio-temporal correlation and multivariate time series prediction, *Int. J. Intell. Syst.* (2021).
- [21] Y. Xiao, K. Xia, H. Yin, Y.-D. Zhang, Z. Qian, Z. Liu, Y. Liang, X. Li, AFSTGCN: Prediction for multivariate time series using an adaptive fused spatial-temporal graph convolutional network, *Digital Communications and Networks* 10 (2024).
- [22] Olaf Ronneberger, Philipp Fischer, and Thomas Brox, "U-Net: Convolutional Networks for Biomedical Image Segmentation", In the Proceeding of Medical Image Computing and Computer-Assisted Intervention – MICCAI 2015, pp 234–241, 2015.
- [23] V.P. Swaminathan, R. Balasubramani, S. Parvathavarthini, V. Gopal, K. Raju, T. S. Sivalingam, S.R. Thennarasu, GAN Based Image Segmentation and Classification Using Vgg16 for Prediction of Lung Cancer, *Journal of Advanced Research in Applied Sciences and Engineering Technology* 35 (1) (2024) 45–61.
- [24] S.A. Althubiti, S. Paul, R. Mohanty, S.N. Mohanty, F. Alenezi, K. Polat, Ensemble learning framework with GLCM texture extraction for early detection of lung cancer on CT images, *Comput. Math. Methods Med.* (2022).
- [25] P.M. Shakeel, M.A. Burhanuddin, M.I. Desa, Automatic lung cancer detection from CT image using improved deep neural network and ensemble classifier, *Neural Comput. & Applic.* (2022) 1–14.
- [26] N. Venkatesan, S. Pasupathy, B. Gobinathan, An efficient lung cancer detection using optimal SVM and improved weight-based beetle swarm optimization, *Biomed. Signal Process. Control* 88 (2024).
- [27] The LIDC-IDRI database will be taken from "<https://wiki.cancerimagingarchive.net/display/Public/LIDC-IDRI>" accessed on May 2024.
- [28] The IQ-OTH/NCCD - Lung Cancer Dataset will be taken from "<https://www.kaggle.com/datasets/adityamahimkar/iqothnccd-lung-cancer-dataset?select=The+IQ-OTHNCCD+lung+cancer+dataset>", accessed on November 2024.
- [29] J.S. Ren, L. Xu, Q. Yan, W. Sun, Shepard convolutional neural networks, *Adv. Neural Inf. Proces. Syst.* 28 (2015).
- [30] N. Siddique, S. Paheeding, C.P. Elkin, V. Devabhaktuni, U-net and its variants for medical image segmentation: A review of theory and applications, *IEEE Access* 9 (2021) 82031–82057.
- [31] A. Banerjee, N. Das, K.C. Santosh, Weber local descriptor for image analysis and recognition: a survey, *Vis. Comput.* 38 (1) (2022) 321–343.
- [32] Roobaert, D., Karakoulas, G. and Chawla, N.V., "Information gain, correlation and support vector machines", In Feature extraction: Foundations and applications, pp. 463–470, Berlin, Heidelberg: Springer Berlin Heidelberg, 2006.
- [33] P. Chinniah, B. Maram, P. Velrajkumar, C. Vidyadhari, DeepJoint Segmentation-based Lung Segmentation and Hybrid Optimization-Enabled Deep Learning for Lung Nodule Classification, *Int. J. Pattern Recognit Artif Intell.* 36 (13) (2022) 2252021.
- [34] K.C. Fan, T.Y. Hung, A novel local pattern descriptor—local vector pattern in high-order derivative space for face recognition, *IEEE Trans. Image Process.* 23 (7) (2014) 2877–2891.
- [35] F. Wu, W. Yang, L. Xiao, J. Zhu, Adaptive wiener filter and natural noise to eliminate adversarial perturbation, *Electronics* 9 (10) (2020) 1634.
- [36] V. Lessa, M. Marengoni, in: *Applying Artificial Neural Network for the Classification of Breast Cancer Using Infrared Thermographic Images*, Springer International Publishing, 2016, pp. 429–438.